Research Square

Preprints are preliminary reports that have not undergone peer review.
They should not be considered conclusive, used to inform clinical practice,
or referenced by the media as validated information.

Curcumin-Loaded pH-Responsive PLGA Nanoparticles Drive Transcriptional Reprogramming of Tumour-Educated Macrophages at Sub- Micromolar Doses in Triple-Negative Breast Cancer

Keerthana Suresh Kizhakkanoodan[1]
Manipal Institute of Technology, Manipal Academy of Higher Education
Sindhura Lakshmi Koulmane Laxminarayana
Kasturba Medical College, Manipal
Deepali Vengala
Manipal Institute of Technology, Manipal Academy of Higher Education
Nithya Swarandika Sappani
Manipal Institute of Technology, Manipal Academy of Higher Education
Kanive Parashiva Guruprasad
Manipal School of Life Sciences, Manipal Academy of Higher Education
Bharath Raja Guru
bharath.guru@manipal.edu

Manipal Institute of Technology, Manipal Academy of Higher Education

Research Article

Keywords: Curcumin, PLGA nanoparticles, Tumour-associated macrophages, Macrophage polarisation, NF-κB, Triple-negative breast cancer

Posted Date: November 25th, 2026

DOI: https://doi.org/10.21203/rs.3.rs-11774578/v1

License: This work is licensed under a Creative Commons Attribution 4.0 International License.
Read Full License

Additional Declarations: No competing interests reported.

Curcumin-Loaded pH-Responsive PLGA Nanoparticles Drive Transcriptional Reprogramming of Tumour-Educated Macrophages at Sub-Micromolar Doses in Triple-Negative Breast Cancer

Keerthana Suresh Kizhakkanoodan[1], Sindhura Lakshmi Koulmane Laxminarayana[2], Deepali Vengala[1], Nithya Swarandika Sappani[1], Kanive Parashiva Guruprasad[3], Bharath Raja Guru[1]*

[1]Manipal Institute of Technology (MIT), Manipal Academy of Higher Education, Manipal, Karnataka 576104, India
[2]Department of Pathology, Kasturba Medical College, Manipal Academy of Higher Education, Manipal, India
[3]Department of Ageing Research, Manipal School of Life Sciences, Manipal Academy of Higher Education, Manipal, India.

Corresponding author: Bharath Raja Guru, bharath.guru@manipal.edu

ORCID (corresponding author): Bharath Raja Guru 0000-0003-2542-7740

Abstract

Tumour-associated macrophages (TAMs) in triple-negative breast cancer (TNBC) are immunosuppressive and promote progression and therapy resistance. Curcumin can repolarise TAMs, but poor solubility and rapid degradation limit its use. We prepared curcumin-loaded poly(lactic-co-glycolic acid) nanoparticles (Cur-PLGA NPs) and studied them in RAW 264.7 macrophages. *In vitro* release was biphasic, with a similar ~19% burst at pH 7.4, 6.4 and 4.5 followed by a slower, pH-dependent phase, reaching about 45% at endolysosomal pH 4.5 versus a plateau near 36% at pH 7.4. Optimised 0.25 μM curcumin, the sub-micromolar dose was used for all treatments. Cur-PLGA NPs treated on macrophages were taken up 2.3–4.4-fold more than free curcumin from 4 h onwards. Two tumour-education models were compared. Transwell co-culture with 4T1 cells raised arginase-1 (ARG1) 34.1-fold but not tumour necrosis factor-α (TNF-α) and gave the lowest CD86:CD206 ratio (0.71), an M2-dominant profile. 4T1-conditioned medium (4T1-CM) raised ARG1 3.50-fold yet gave the highest ratio (1.24 versus 0.77 in control), a hybrid profile resembling that reported for TNBC TAMs. In 4T1-CM-educated macrophages, free curcumin and Cur-PLGA NPs both raised TNF-α (5.5- and 5.8-fold) and lowered ARG1. The CD86:CD206 ratio also rose with both, driven by CD86. In the same model, *Nfkb1* transcript rose 2.76-fold with 4T1-CM and further after treatment, 4.7-fold with free curcumin and 17.2-fold with Cur-PLGA NPs. The stronger nanoparticle response is consistent with their greater uptake. Together, these changes indicate attenuation of the immunosuppressive signature at a sub-micromolar dose, positioning Cur-PLGA NPs as a macrophage-directed platform for TNBC.

Keywords Curcumin; PLGA nanoparticles; Tumour-associated macrophages; Macrophage polarisation; NF-κB; Triple-negative breast cancer

1. Introduction

Triple-negative breast cancer (TNBC), defined by the absence of oestrogen receptor, progesterone receptor and HER2 expression, accounts for roughly 15–20% of breast cancers, the most frequently diagnosed malignancy and leading cause of cancer death in women worldwide (Bray et al. 2024). TNBC metastasises early, offers few actionable molecular targets and shows limited durable responses to chemotherapy (Yin et al. 2020), making the tumour immune microenvironment an attractive therapeutic target.

Tumour-associated macrophages (TAMs) are the most abundant non-malignant infiltrating cells in the tumour microenvironment. Driven by tumour-derived signals such as colony-stimulating factor 1, interleukin-10 (IL-10), TGF-β1 and prostaglandin E2, they predominantly adopt immunosuppressive, pro-angiogenic M2-like phenotypes (Qian and Pollard 2010; Biswas and Mantovani 2010), and high TAM density correlates with metastasis, chemoresistance and poor survival in TNBC (Murdoch et al. 2008; Cassetta and Pollard 2023). In established TNBC, however, TAMs rarely occupy discrete M1 or M2 states. They co-express M1-associated markers (CD86, tumour necrosis factor-α [TNF-α], nuclear factor-κB [NF-κB]) and M2-associated markers (CD206, arginase-1 [ARG1], TGF-β1), and their M1 programme is often partial, with NF-κB and CD86 upregulation not extending to effector cytokines such as TNF-α (Mosser and Edwards 2008; Italiani and Boraschi 2014; Martinez and Gordon 2014; Pe et al. 2022; Wu and Liao 2025). Reprogramming TAMs towards a tumoricidal M1-like phenotype is therefore a rational therapeutic strategy (Murray et al. 2014; Weagel et al. 2015; Cassetta and Pollard 2023).

Classical M1 polarisation is driven by NF-κB (p65/p50) and interferon regulatory factor 5, which transactivate TNF-α, IL-1β, inducible nitric oxide synthase and CD86 (Liu et al. 2017), whereas STAT6, IRF4 and KLF4 downstream of IL-4/IL-13 induce ARG1, CD206, IL-10 and TGF-β1 (Lawrence and Natoli 2011). Tumour-derived signals can engage both axes simultaneously, generating hybrid phenotypes whose composition varies with the tumour secretome (Steenbrugge et al. 2018).

Curcumin, the principal polyphenol of *Curcuma longa*, modulates NF-κB in a context-dependent manner, inhibits STAT6 and PI3Kγ/δ signalling and epigenetically remodels macrophage gene promoters (Menon and Sudheer 2007; Hagemann et al. 2008; Aggarwal and Harikumar 2009; Connelly et al. 2011; Deswal et al. 2024). In M2-polarised and tumour-conditioned macrophages, it can enhance NF-κB-dependent pro-inflammatory output while suppressing the IL-4/STAT6–ARG1 axis, a mechanism distinct from its anti-inflammatory activity in hyper-stimulated M1 cells (Shiri et al. 2015; Jiang et al. 2022). Its pharmacological use is, however, limited by poor aqueous solubility (≤11 ng/mL at physiological pH), rapid degradation, ~1% oral bioavailability and efflux from phagocytic cells (Anand et al. 2007; Yallapu et al. 2012).

Encapsulation in poly (lactic-co-glycolic acid) (PLGA), an FDA-approved biodegradable copolymer, offers a way around these limitations (Astete and Sabliov 2006; Makadia and Siegel 2011; Kizhakkanoodan et al. 2023; Paladugulu et al. 2025).

PLGA nanoparticles are internalised by macrophages and routed to acidic (pH 4.5–5.0) endolysosomes, where accelerated polymer hydrolysis favours intracellular drug release (Galloway et al. 1983). pH-gated nanoparticles have been used to repolarise TAMs (Tang et al. 2023), and curcumin co-encapsulation has been explored in breast cancer (Praveena et al. 2025) and other solid tumour cell lines (Praveena et al. 2022).

Curcumin has been shown to reprogramme macrophages already educated by tumour-conditioned medium or co-culture at 5–20 μM (Jiang et al. 2022); whether this occurs in TNBC-educated macrophages with a hybrid phenotype, and at sub-micromolar, non-cytotoxic concentrations achievable with nanoparticle delivery, is less clear. Here, free curcumin (Cur-FD) and curcumin-loaded PLGA nanoparticles (Cur-PLGA NPs) were compared for their ability to shift macrophages educated by 4T1 TNBC-conditioned medium (4T1-CM) from a hybrid towards an M1-like phenotype. The study integrates physicochemical characterisation, pH-dependent release, concentration–response cytotoxicity, quantitative and confocal uptake, and transcriptional, surface-marker, oxidative and functional readouts within a single experimental framework.

2. Materials and Methods

2.1 Materials

Poly(lactic-co-glycolic acid) (PLGA 50:50, average MW 65-95 kDa), poly (vinyl alcohol) (PVA), and dimethyl sulfoxide (DMSO) were purchased from Sigma-Aldrich (St. Louis, MO, USA). Curcumin (MW 368.38 g/mol; 95% total curcuminoid content; cat. no. B21573), CellTracker™ Red CMTPX (MW 686.3 g/mol), and 2′,7′-dichlorodihydrofluorescein diacetate (H2DCFDA, DCFH-DA) were obtained from Thermo Fisher Scientific (Waltham, MA, USA). HPLC-grade acetonitrile, chloroform, isopropanol and methanol were procured from Merck Life Science Pvt. Ltd. (Mumbai, India); trifluoroacetic acid (TFA) and Tween 80 were obtained from Loba Chemie Pvt. Ltd. (Mumbai, India). Dulbecco's Modified Eagle Medium (DMEM), fetal bovine serum (FBS), antibiotic-antimycotic solution, Phenol-red free Trypsin 2.5% Solution 10X, Bradford reagent, cell culture-grade DMSO, and MTT [3-(4,5-dimethylthiazol-2-yl)-2,5-diphenyltetrazolium bromide], 4% Paraformaldehyde in Phosphate Buffered Saline were purchased from HiMedia Laboratories Pvt. Ltd. (Mumbai, India). Lipopolysaccharide (LPS; Escherichia coli O111:B4, γ-irradiated, BioXtra) and recombinant murine interleukin-4 (IL-4, lyophilised) were obtained from Sigma-Aldrich. Semi-transparent cell culture inserts were from HiMedia Laboratories Pvt. Ltd. (Mumbai, India). Primescript RT Reagent Kit (Perfect real-time), TBGreen Premix Ex Taq II (Tli RNaseH Plus) were purchased from Takara, Kusatsu, Shiga, Japan.

For flow cytometric immunophenotyping, fluorochrome-conjugated anti-mouse monoclonal antibodies were used: CD14-FITC, CD11b-PE, CD86-PE-Cy7, and CD64-APC (Thermo Fisher Scientific/Invitrogen, Waltham, MA, USA); CD206-PerCP-Cy5.5 (BioLegend, San Diego, CA, USA); and CD45-V500 (BD Biosciences, Franklin Lakes, NJ, USA). The murine macrophage cell line RAW 264.7 was procured from the National Centre for Cell Science (NCCS, Pune, India). The murine breast cancer cell line 4T1 was a kind gift from Dr. K. Nanda Kumar (Manipal College of Pharmaceutical Sciences, MAHE, India).

2.2 Preparation of Cur-PLGA Nanoparticles

Cur-PLGA NPs (labelled Cur-NP in figures) were prepared by the single-emulsion solvent evaporation method. Curcumin was dissolved in 2 mL of chloroform by sonication followed by the addition of PLGA to maintain a 2:1 polymer-to-drug ratio. The organic phase was added dropwise to 12 mL chilled 2% (w/v) PVA and emulsified under ice-cold conditions by probe sonication at 40% amplitude for 6 min (1-min pause at 3 min; Qsonica Q700, Newtown, CT, USA). The emulsion was stirred magnetically overnight for complete solvent evaporation. The nanoparticle suspension was centrifuged at 16,000 × g for 40 min (Eppendorf 5804R), washed three times with chilled deionised water with intermediate bath sonication, frozen at −80 °C overnight, lyophilised for 48 h (Labogene Scanvac CoolSafe), and stored at −20 °C. All steps were performed under subdued light.

2.3 Physicochemical Characterisation

Hydrodynamic diameter and polydispersity index (PDI) were determined by dynamic light scattering (DLS), and zeta potential by electrophoretic light scattering, using a Zetasizer Nano ZS (ZEN 3600, Malvern Instruments, UK) at 25 °C with NPs dispersed in deionised water. Surface morphology was examined by field-emission scanning electron microscopy (FE-SEM; JSM-7610FPlus, JEOL, Japan) at 5.0 kV and 30,000× magnification; samples were gold-sputter-coated before imaging. Drug loading was quantified by reverse-phase high-performance liquid chromatography (RP-HPLC) (Shimadzu

LC-20AD, SPD-20A, SIL-20AC HT, Japan) using a Kinetex eVO C18 column (250 × 4.6 mm, 5 µm, 100 Å) with isocratic acetonitrile:water (70:30, v/v) + 0.01% TFA, detected at 370 nm. Lyophilised NPs (1 mg) were dissolved in methanol, rocked for 48 h, pelleted by centrifugation, and the supernatant was evaporated and reconstituted in 1 mL HPLC-grade acetonitrile for injection. Drug loading is expressed as µg curcumin per mg NP. The HPLC method was adapted from previously validated protocols for simultaneous estimation and stability analysis of curcumin in nanoformulations (Supplementary material, Figs. S1 and S2) (Praveena and Guru 2021).

2.4 In Vitro Drug Release

Release was evaluated at pH 7.4 (PBS; systemic circulation), 6.4 (PBS; intratumoral interstitium) and 4.5 (citrate buffer; endolysosomal compartment) over 30 days (720 h). Cur-PLGA NPs (1 mg; drug loading 279.91 ± 33.32 µg curcumin/mg NP) were dispersed in 1 mL of the respective buffer supplemented with 0.5% (w/v) Tween 80 to maintain pseudo-sink conditions and incubated at 37 °C with shaking, in triplicate (n = 3 per pH). At predetermined time points (0.5–720 h), vials were centrifuged (16,000 × g, 10 min), and 250 µL of supernatant was withdrawn and replaced with an equal volume of fresh buffer. The aliquot was evaporated to dryness, reconstituted in 250 µL acetonitrile, filtered through a 0.22 µm membrane and quantified by RP-HPLC. Cumulative release was calculated as $Q_n = C_nV + v\sum_{i=1}^{n-1}C_i$, where C_n is the curcumin concentration at the nth sampling, V is the release volume (1 mL) and v is the sampled volume (0.25 mL) and expressed as a percentage of the total curcumin loaded. One pH 4.5 sample at 10 h returned an aberrant concentration (95.1 µg/mL vs. ~41 µg/mL in the other replicates and adjacent timepoints) and was excluded as a technical failure; for the sampling correction of subsequent timepoints, its concentration was replaced by the mean of the adjacent (8 h and 12 h) values. Release data are reported from 2 h onward; the 0.5 h sample was included in the cumulative correction.

2.5 Cell Lines and Culture

RAW 264.7 murine macrophages (Raschke et al. 1978) and 4T1 murine TNBC cells were maintained in DMEM supplemented with 10% heat-inactivated FBS and 1% antibiotic-antimycotic solution at 37°C in a 5% CO_2 humidified atmosphere. Cells were passaged at 70-80% confluence.

2.6 Cell Viability (MTT Assay)

RAW 264.7 cells were seeded at 1×10^4 cells/well in 96-well plates and allowed to adhere overnight. Cells were treated with free curcumin (Cur-FD) or Cur-PLGA NPs at 0, 0.25, 0.5, 1, 2, 3, and 5 µM (curcumin-equivalent) in phenol red-free, serum-deprived medium for 24, 48, and 72 h, with concentration-matched blank wells to account for curcumin's inherent colour. After incubation, MTT working solution (0.5 mg/mL in DMEM) was added and plates were incubated for 4 h at 37°C. The medium-MTT mixture was discarded, formazan crystals were solubilised in DMSO (100 µL), and absorbance was measured at 570/630 nm (Thermo Fisher Varioskan LUX 3020). Viability is expressed as percentage of untreated control after blank subtraction. Five independent experiments were performed, each with six technical replicate wells per condition. Outlying values, predominantly near-zero or negative readings indicating technical failure, were identified by the ROUT method (Q = 1%) and excluded prior to analysis; twelve of 210 values were removed (nine at 24 h, two at 48 h, one at 72 h), giving n = 3–5 per condition. All excluded values are itemised in Supplementary material, Table S1.

2.7 Quantitative Cellular Uptake

RAW 264.7 cells (6×10^5/well) were treated with 20 µM curcumin-equivalent Cur-FD or Cur-PLGA NPs for 0.5, 2, 4, 6, and 12 h (n = 3 independent biological replicates per timepoint); this higher concentration was used to obtain quantifiable intracellular curcumin fluorescence over the short exposure periods. Cells were washed with PBS, pelleted (16,000 × g, 10 min), and stored at −80 °C. Intracellular curcumin was extracted by three freeze-thaw cycles followed by bath sonication for 15 min. Cell pellets were resuspended in 500 µL PBS; 250 µL was reserved for Bradford protein quantification and the remaining 250 µL was mixed 1:1 with methanol and centrifuged. Curcumin in the supernatant was quantified by fluorescence (λ ex/em: 430/530 nm; Varioskan LUX 3020) against a calibration curve prepared in the same solvent, and a dilution factor of 2.0 was applied to correct for the 1:1 methanol addition. Values were converted to molar units using the molecular weight of curcumin (368.38 g/mol), normalised to total protein content, and expressed as nmol curcumin per mg protein (replicate-level data in Supplementary material, Table S2).

2.8 Qualitative Cellular Uptake by Confocal Microscopy

RAW 264.7 cells (7×10^4/well) were seeded in SPL Cell Culture Slide I confocal chambers (FBS-treated glass) and treated with 20 µM curcumin-equivalent Cur-FD or Cur-PLGA NPs for 2 h. A higher concentration and short exposure were used to obtain sufficient curcumin fluorescence for imaging; no morphological signs of cytotoxicity were observed at 2 h. Cells were sequentially stained with CellTracker™ Red CMTPX (1 µM, 20 min) and Hoechst 33342 (1 µg/mL, 5 min) in serum-free medium, exploiting curcumin's intrinsic green autofluorescence (λ_{ex} 498 nm, λ_{em} 517 nm) for drug localisation without a chemical conjugate. Cells were washed, mounted with a coverslip, and imaged using an Olympus FV5000 confocal laser scanning microscope (100× oil-immersion objective). Cells exposed to blank (curcumin-free) PLGA nanoparticles were stained identically and imaged in the brightfield, Hoechst and CellTracker Red channels (Supplementary material, Fig. S3). Merged images were generated by additive overlay of the fluorescence channels; no non-linear adjustments were applied.

2.9 4T1 Conditioned Medium Preparation and Macrophage Polarisation

4T1 conditioned medium (4T1-CM) was prepared by washing 4T1 cells at ~30% confluency three times with PBS, followed by 48 h incubation in DMEM containing 2% FBS. The collected supernatant was centrifuged (300 × g, 5 min, 4°C) and filtered through a 0.22 µm membrane to yield sterile 4T1-CM. RAW 264.7 macrophages were stimulated for 48 h under: (i) vehicle control (DMEM + 10% FBS); (ii) M1 polarisation (LPS, 100 ng/mL); (iii) M2 polarisation (IL-4, 40 ng/mL); (iv) tumour education (4T1-CM, 1:1 dilution); or (v) transwell indirect co-culture (RAW 264.7:4T1, 1:3 ratio, 0.4 µm pore). For repolarisation, macrophages were first conditioned with 4T1-CM for 48 h, washed three times with PBS, then treated with 0.25 µM Cur-FD (DMSO ≤ 0.1%) or Cur-PLGA NPs for a further 48 h. The 0.25 µM concentration was selected from the MTT concentration–response (Section 3.3) as the concentration at which both formulations maintained ≥85% viability at every time point.

2.10 Macrophage Morphometry

RAW 264.7 macrophages were co-cultured with 4T1 cells in a transwell system at RAW 264.7:4T1 ratios of 1:1, 1:2, 1:3, and 1:4 for 48 h, with RAW 264.7 monoculture as control. Phase-contrast micrographs (20×) were acquired from 3 random fields per condition (10 cells per field; N = 30 per condition) from a single representative experiment. Cell outlines were traced manually, and the minimum diameter (cellSens "Diameter (min.)": the shortest line through the cell centroid connecting two points on the traced outline) was measured using CellSens Standard software (Olympus Corporation) and converted to µm with a calibrated scale bar. Diameters are reported as mean ± SD of all annotated cells (N = 30 per condition). Because all fields derive from a single experiment and represent technical rather than biological replicates, statistical comparisons (one-way ANOVA with unadjusted pairwise Welch's t-tests, Supplementary material, Table S3) are exploratory and describe within-experiment differences only. This titration was performed to select the co-culture ratio used in subsequent experiments. Representative micrographs and full morphometric data are provided in Supplementary material, Fig. S4 and Table S3.

2.11 RT-qPCR

Total RNA was extracted using TRIzol reagent followed by cold chloroform phase separation (12,000 × g, 15 min, 4 °C). The aqueous phase was precipitated with isopropanol, the pellet washed twice with 70% ethanol, air-dried, and dissolved in DEPC-treated water. RNA purity was assessed at A260/A280. Reverse transcription was performed with the PrimeScript RT Reagent Kit (Takara Bio, Japan). RT-qPCR was performed on a Bio-Rad CFX96 system using TB-Green Premix Ex Taq II (Takara Bio) with ROX as passive reference dye. Primer sequences are listed in Table 1. β-Actin (Actb) served as the housekeeping reference gene. Relative expression was quantified by the 2^−ΔΔCq method (Livak and Schmittgen 2001), following the MIQE recommendations, where applicable, for the reporting of quantitative real-time PCR experiments (Bustin et al. 2009).

Independent biological replicates were performed as follows: n = 5 for TNF-α and ARG1 in the polarisation experiments, and n = 3 for NF-κB and for all repolarisation experiments. ΔCq values were screened for outliers by the ROUT method (Q = 1%); no outliers were identified, and all values were retained (ΔCq values for all replicates are provided in Supplementary material, Table S4).

All statistical comparisons were performed on ΔCq values, which are already on a logarithmic scale, using repeated-measures one-way ANOVA with Geisser–Greenhouse correction for departure from sphericity, followed by Tukey's post-hoc test. Fold-changes are reported as geometric means, appropriate for ratio data, with 95% confidence intervals obtained by back-transformation of the corresponding ΔCq differences. Transwell co-culture samples were processed in separate

qPCR runs, each containing its own matched 48 h control, and were therefore analysed independently as paired within-run comparisons using a one-sample t-test against ΔΔCq = 0. Co-regulation of TNF-α and ARG1 was assessed by Spearman rank correlation of ΔΔCq values across treatment conditions; values for the reference condition, which equal zero by definition, were excluded. To validate the sequential 48 h → 96 h experimental design, untreated macrophages were harvested in parallel at 48 h (C48h) and 96 h (C96h; untreated, and distinct from the 4T1-CM-primed C96 reference used for flow cytometry and ROS in Sections 2.12–2.13) and compared by paired t-tests with intraclass correlation coefficients.

Table 1 Primer sequences used for RT-qPCR analysis of macrophage polarisation markers.

Gene	Forward primer (5'→3')	Reverse primer (5'→3')	Function
TNF-α (*Tnf*)	CCCCAAAGGGATGAGAAGTT	CACTTGGTGGTTTGCTACGA	M1 marker
ARG1 (*Arg1*)	CATTGGCTTGCGAGACGTAGAC	GCTGAAGGTCTCTTCCATCACC	M2 marker
NF-κB (*Nfkb1*)	CCGTCTGTCTGCTCTCTCT	CGTAGGGATCATCGTCTGCC	M1 transcription factor
β-Actin (*Actb*)	GTGCTATGTTGCTCTAGACTTCG	ATGCCACAGGATTCCATACC	Reference gene

2.12 Flow Cytometry

Macrophages were harvested by gentle scraping, washed with PBS and pelleted (400 × g, 5 min). Cell pellets were stained for 15 min at room temperature in the dark with CD45-V500 (clone 30-F11; BD Horizon, cat. no. 561487; 5 µL), CD64-APC (clone X54-5/7.1; Thermo Fisher Scientific, cat. no. 17-0641-80; 5 µL), CD86-PE-Cy7 (clone GL1; Thermo Fisher Scientific, cat. no. 25-0862-80; 2.5 µL) and CD206-PerCP-Cy5.5 (clone C068C2; BioLegend, cat. no. 141715; 2.5 µL). CD14-FITC (2.5 µL) and CD11b-PE (2.5 µL) were also included in the staining panel but were not used for gating or analysis. Cells were washed with 2 mL PBS (300 × g, 5 min), resuspended in 500 µL PBS and acquired unfixed on a BD FACSCanto II flow cytometer using BD FACSDiva software v8.0.3.

Unstained cells were used as negative controls to define positive gates. A total of 100,000 events were acquired per sample. Doublets were excluded on FSC-H vs. FSC-A, cells were gated on FSC-A vs. SSC-A, and macrophages were identified as $CD64^{+}CD45^{+}$. Within the macrophage gate, the median fluorescence intensity (MFI) of CD86 and CD206 was recorded for each sample. The CD86:CD206 MFI ratio was used as a composite M1/M2 polarisation index (interpreted relative to the unstimulated control, as CD86 and CD206 are detected with different fluorochromes and a ratio of 1.0 is therefore not a meaningful threshold). The gating strategy is shown in Supplementary material, Fig. S5, and replicate-level MFI values are given in Supplementary material, Table S5. Three independent biological replicates were analysed per group.

2.13 Intracellular ROS (DCFH-DA Assay)

Intracellular ROS, a key oxidative effector in macrophage-mediated immune signalling (Schieber and Chandel 2014), was quantified using the DCFH-DA assay. Cells were washed and incubated with 20 µM DCFH-DA in serum-free medium for 30 min at 37°C in the dark. Cells were collected by scraping and centrifuged (300 × g, 5 min, 4°C). Fluorescence was measured in triplicate from 100 µL cell suspension in a black 384-well plate (λex/em 485/530 nm; Varioskan LUX 3020). The remaining aliquot was used for Bradford protein quantification. Raw fluorescence values were blank-subtracted and normalised to protein concentration (RFU/µg protein). Results are expressed as fold change relative to the unstimulated 48 h control (C48; polarisation, n = 5) or, for the repolarisation arm, a matched 4T1-CM-primed, vehicle-treated 96 h control (C96: 48 h 4T1-CM priming followed by 48 h of the same vehicle used for the curcumin formulations, without curcumin; n = 3) — a full-duration reference distinct from the 48 h 4T1-CM timepoint reused as the qPCR repolarisation reference (Section 2.11). One C96 value from a single acquisition was excluded as a technical outlier (0.0059 RFU/µg

protein vs. 0.021–0.040 in the other three C96 samples; >2 SD below their mean); that experiment was therefore excluded in its entirety, as disclosed in Supplementary material, Table S6.

2.14 Scratch Wound Healing Assay

Macrophage-conditioned media were obtained from RAW 264.7 macrophages polarised for 48 h under M1 (LPS), M2 (IL-4) or tumour-educating (4T1-CM) conditions (Section 2.9). At the end of polarisation, the culture medium was collected directly, centrifuged and filtered as described for 4T1-CM (Section 2.9), and designated M1-conditioned medium (M1-CM), M2-conditioned medium (M2-CM) and conditioned medium from tumour-educated macrophages (TAM-CM), respectively. 4T1 cells grown to confluence were scratched using a 200 µL pipette tip, washed twice with PBS, and incubated with M1-CM, M2-CM, TAM-CM or 4T1-CM, alongside DMEM + 10% FBS (positive control) and DMEM + 1% FBS (negative control). All conditioned media, including 4T1-CM, were applied directly (undiluted) to the scratched monolayers. Because the polarising stimuli were not removed before collection, M1-CM and M2-CM also contained residual LPS and IL-4, and TAM-CM contained residual 4T1-derived factors; 4T1-CM applied directly to 4T1 cells was therefore included as a carry-over control to distinguish macrophage-derived effects from those of the tumour-conditioned medium itself. Phase-contrast images (10× objective) were captured at 0 h and 24 h. Scratch width was measured at three equally spaced positions perpendicular to the wound in each field using CellSens Standard software (Olympus Corporation), and the mean width (W) was used to calculate percentage wound closure as $[(W_0 - W_{24})/W_0] \times 100$. Eight independent biological replicates were performed per group (n = 8). Group differences were assessed by the Kruskal-Wallis test (non-parametric one-way ANOVA), followed by Dunn's multiple comparisons test for pairwise comparisons among the six groups. A functional migration/wound-healing assay was not performed for the repolarisation arm (Section 2.9); the rationale is given in Section 4.4.

2.15 Statistical Analysis

Statistical analyses were performed in GraphPad Prism 10.6, and $p < 0.05$ was considered statistically significant. In vitro release: cumulative release at 2 h and 30 days was compared between pH conditions by ordinary one-way ANOVA with Tukey's multiple comparisons test; homogeneity of variances was confirmed with the Brown–Forsythe test ($p > 0.05$). MTT cytotoxicity: two-way ANOVA with Dunnett's multiple comparisons test against untreated control; outliers removed by ROUT (Q = 1%). Cellular uptake: two-way repeated-measures ANOVA with Šídák-corrected pairwise comparisons between formulations at each timepoint (5 comparisons). RT-qPCR: repeated-measures one-way ANOVA (Geisser–Greenhouse) with Tukey's post-hoc test; one-sample t-test against $\Delta\Delta Cq = 0$ for the transwell co-culture comparison. Flow cytometry (MFI and CD86:CD206 ratio) and intracellular ROS: ordinary one-way ANOVA with Tukey's post-hoc test; one-sample t-tests against 1.0 for fold-change ROS data and Welch's t-test for the Cur-FD vs. NP comparison. Wound healing: Kruskal–Wallis test with Dunn's multiple comparisons test. Effect sizes: Cohen's d where reported (small < 0.5, medium 0.5-0.8, large > 0.8). Spearman ρ for gene co-expression correlation. Post-hoc power was estimated using the non-central t-distribution at $\alpha = 0.05$ (two-tailed). Statistical significance: * $p < 0.05$, ** $p < 0.01$, *** $p < 0.001$, **** $p < 0.0001$. A consolidated summary of statistical approaches by assay is provided in Supplementary material, Note S1.

3. Results

3.1 Physicochemical Characterisation of Cur-PLGA Nanoparticles

Cur-PLGA NPs were prepared by single-emulsion solvent evaporation, yielding a lyophilised powder readily reconstituted in aqueous media (Table 2). DLS showed a Z-average diameter of 240.5 nm with a narrow size distribution (PDI 0.076). The moderately negative zeta potential (−12.3 mV) reflects residual anionic PLGA carboxyl end groups, with colloidal stability provided mainly by PVA steric stabilisation, consistent with published PLGA–PVA systems (Astete and Sabliov 2006; Makadia and Siegel 2011). FE-SEM showed predominantly spherical particles (Fig. 1), with individual dry-state diameters of 140–307 nm spanning the DLS Z-average; occasional plate-like crystals, likely unencapsulated curcumin or excipient residue, were also observed. RP-HPLC confirmed curcumin encapsulation (main peak at 3.29 min; Supplementary material, Figs. S1–S2), with a drug loading of 279.91 ± 33.32 µg curcumin/mg NP.

Table 2 Physicochemical properties of curcumin-loaded PLGA nanoparticles (Cur-PLGA NPs). DLS = dynamic light scattering; FE-SEM = field-emission scanning electron microscopy; RP-HPLC = reverse-phase high-performance liquid chromatography.

Parameter	Value
Z-average diameter (DLS)	240.5 nm
Polydispersity index (PDI)	0.076
Zeta potential	−12.3 mV (zeta deviation 5.79 mV)
Dry-state diameter range (FE-SEM)	140–307 nm
Morphology (FE-SEM)	Predominantly spherical
Drug loading (RP-HPLC)	279.91 ± 33.32 µg curcumin/mg NP
HPLC retention time	3.29 min (370 nm)

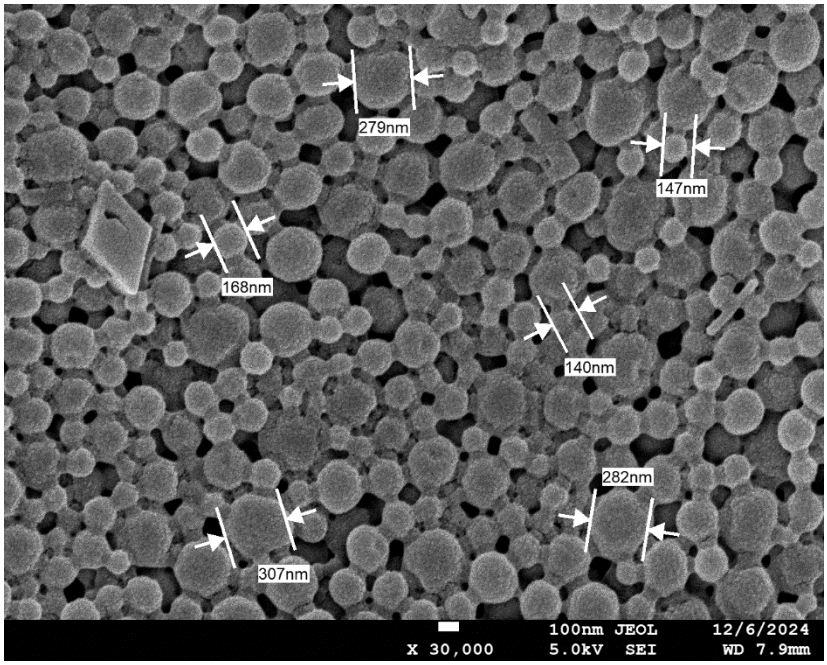


Fig. 1 FE-SEM micrograph of Cur-PLGA NPs (JEOL JSM-7610FPlus; 30,000×, 5.0 kV; gold-sputter-coated; scale bar = 100 nm) showing predominantly spherical particles. Representative particle diameters (140–307 nm) are indicated.

3.2 In Vitro Drug Release: Biphasic, pH-Dependent Release with Drug Retention

Curcumin release from Cur-PLGA NPs over 30 days (720 h) showed a biphasic profile at all three pH values (Fig. 2). An initial burst release of 19.73 ± 0.47%, 18.65 ± 0.96% and 19.12 ± 0.31% occurred within 2 h at pH 7.4, 6.4 and 4.5, respectively, and did not differ between pH conditions (one-way ANOVA, $p = 0.20$). This burst is attributable to rapid diffusion of surface-adsorbed drug (Roshan et al. 2024). By 24 h, cumulative release had reached 35.75 ± 0.77%, 35.30 ± 0.97% and 39.61 ± 0.45%, respectively (Fig. 2, inset). Thereafter, release at pH 7.4 plateaued at ~36%, whereas release at pH 6.4 and 4.5 continued to increase slowly for approximately 12–14 days (from ~35% to ~38% and from ~40% to ~45%,

respectively). Minor fluctuations in mean values (<2%) were within experimental variability and may reflect partial degradation of curcumin in the release medium.

The release profiles overlapped during the burst phase and diverged from approximately 12–24 h onwards. At 30 days, cumulative release was highest at pH 4.5 (44.58 ± 0.49%), compared with pH 6.4 (38.22 ± 0.48%) and pH 7.4 (35.81 ± 1.16%) (one-way ANOVA, $F(2,6) = 100.9$, $p < 0.0001$). Tukey's post hoc test showed that release at pH 4.5 was significantly higher than at both pH 7.4 ($p < 0.0001$) and pH 6.4 ($p = 0.0001$), and release at pH 6.4 was also modestly but significantly higher than at pH 7.4 ($p = 0.021$). This pH-dependent increase is consistent with accelerated PLGA hydrolysis under acidic conditions (Makadia and Siegel 2011), although the greater chemical stability of curcumin at acidic pH may also contribute to the higher apparent release (Wang et al. 1997; Praveena and Guru 2021). Incomplete release at all pH values (~36–45%) is characteristic of compact PLGA matrices over this time frame (Astete and Sabliov 2006; Makadia and Siegel 2011).

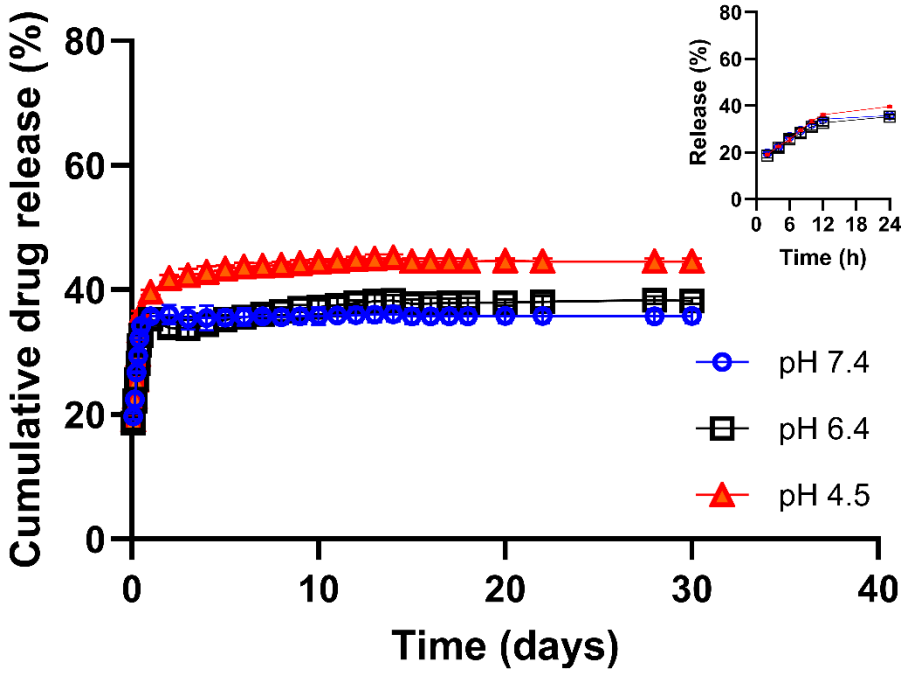


Fig. 2 Cumulative *in vitro* release of curcumin from Cur-PLGA NPs at pH 7.4, 6.4 and 4.5 over 30 days (720 h). Inset: release during the first 24 h, showing an initial burst of ~19% within 2 h at all pH values. Cumulative release at 30 days was significantly higher at pH 4.5 than at pH 7.4 and 6.4 ($p < 0.001$), and at pH 6.4 than at pH 7.4 ($p < 0.05$) (one-way ANOVA with Tukey's post hoc test). Data are mean ± SD (n = 3 independent release vessels per pH; n = 2 for pH 4.5 at 10 h, one technical failure excluded).

3.3 Cytotoxicity of Free Curcumin and Cur-PLGA NPs in RAW 264.7 Macrophages

MTT cytotoxicity was evaluated across 0–5 µM at 24, 48, and 72 h to establish a non-cytotoxic working concentration for the macrophage polarisation experiments, in which cells are exposed to curcumin for 48 h (Fig. 3; full dataset in Supplementary material, Table S1). At the working concentration of 0.25 µM, viability remained ≥85% for both formulations at every timepoint and was 93.79% (Cur-FD) and 87.88% (NPs) at the 48 h exposure duration used downstream; this concentration was therefore selected for all subsequent experiments. Two-way ANOVA identified concentration as the sole significant source of variation at all timepoints (24 h: $F(6,47) = 2.50$, $p = 0.035$; 48 h: $F(6,54) = 2.83$, $p = 0.018$; 72 h: $F(6,55) = 4.18$, $p = 0.002$). The formulation factor (Cur-FD vs. NPs) was non-significant at all timepoints ($p = 0.076$, 0.455, and 0.116 respectively), with no significant concentration × formulation interaction (all $p > 0.14$), indicating that nanoencapsulation did not alter the cytotoxic profile of curcumin. Equimolar comparison of the two formulations in the repolarisation experiments was therefore not confounded by differential viability. Reductions in viability reaching statistical significance versus untreated control (Dunnett's test) occurred only at ≥1 µM, at least four-

fold above the working concentration, and were not consistent across timepoints or formulations (Cur-FD at 1 and 2 μM at 24 h, p = 0.040 and 0.043; Cur-PLGA NPs at 5 μM at 48 h, p = 0.020, and at 3 μM at 72 h, p = 0.027). No concentration ≤0.5 μM differed from control at any timepoint, and viability remained above 50% even at 5 μM, indicating that IC_{50} was not reached within the range tested.

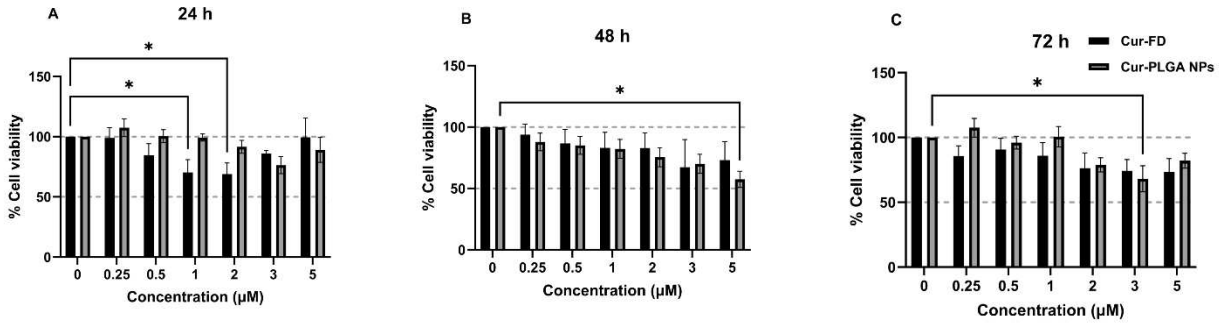


Fig. 3 Dose–response cytotoxicity of free curcumin (Cur-FD) and Cur-PLGA NPs in RAW 264.7 macrophages at (A) 24 h, (B) 48 h and (C) 72 h; 48 h corresponds to the exposure duration used in the polarisation experiments. Data are mean ± SEM (n = 3–5 independent experiments; outliers removed by ROUT, Q = 1%), expressed as percentage of untreated control. Dashed lines indicate 100% and 50% viability. Two-way ANOVA: concentration was significant at all time points; formulation and interaction were not. Dunnett's post-hoc test vs. untreated control within each formulation: *p < 0.05.

3.4 Quantitative Cellular Uptake: Enhanced Intracellular Curcumin Delivery by Cur-PLGA NPs

Cellular uptake of curcumin was quantified in RAW 264.7 macrophages at 0.5, 2, 4, 6, and 12 h at 20 μM curcumin-equivalent (Fig. 4; replicate-level data in Supplementary material, Table S2). Both formulations were detectable from 0.5 h. Free curcumin uptake remained low and largely non-progressive across the time course (8.64–18.06 nmol/mg protein), whereas Cur-PLGA NP uptake (mean ± SD) rose from 14.00 ± 3.53 nmol/mg protein at 0.5 h to 38.25 ± 11.42, 37.29 ± 17.08, and 42.37 ± 8.25 nmol/mg protein at 4, 6, and 12 h respectively, corresponding to 4.4-, 2.6-, and 2.3-fold higher intracellular accumulation than Cur-FD at the matched timepoints.

Two-way repeated-measures ANOVA (matched by both factors, Geisser–Greenhouse corrected) identified a significant main effect of formulation ($F(1,2) = 22.35$, $p = 0.042$), with mean intracellular curcumin of 30.21 nmol/mg protein for Cur-PLGA NPs versus 12.76 nmol/mg protein for Cur-FD across the time course (mean difference 17.45 nmol/mg protein, 95% CI 1.57 to 33.33). The main effect of time ($F(1.08, 2.15) = 9.48$, $p = 0.084$) and the time × formulation interaction ($F(1.26, 2.52) = 7.59$, $p = 0.086$) did not reach significance after correction for a substantial departure from sphericity (ε = 0.27 and 0.32 respectively); both trended towards progressively divergent uptake, and neither these nor the Šídák-corrected pairwise comparisons should be read as absence of effect at n = 3.

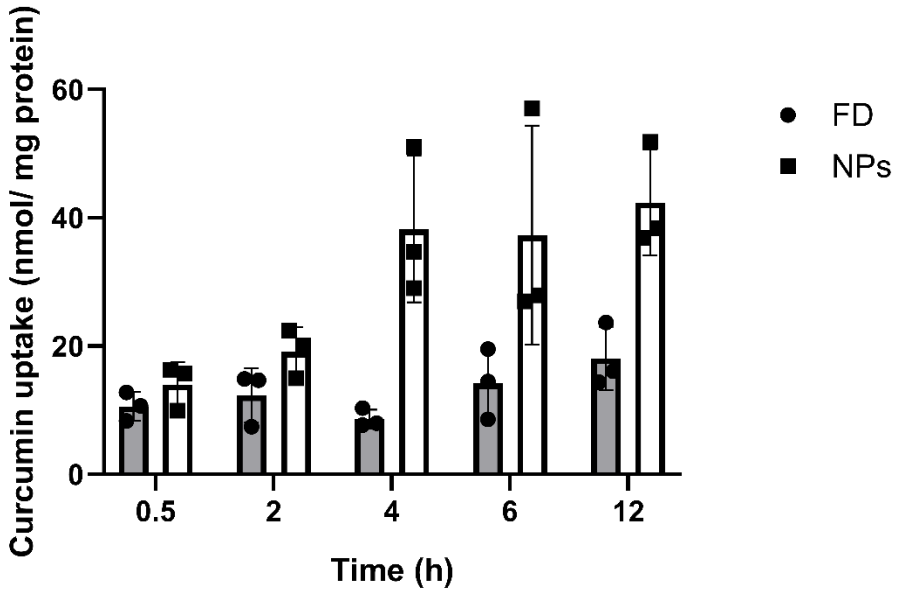


Fig. 4 Cellular uptake of free curcumin (FD) and Cur-PLGA NPs (NPs) in RAW 264.7 macrophages over 12 h, expressed as nmol curcumin per mg cellular protein. Bars represent mean ± SD; individual data points represent independent biological replicates (n = 3 per timepoint). Two-way repeated-measures ANOVA (matched by both factors, Geisser–Greenhouse corrected): formulation $F(1,2) = 22.35$, $p = 0.042$; time $F(1.08, 2.15) = 9.48$, $p = 0.084$; time × formulation interaction $F(1.26, 2.52) = 7.59$, $p = 0.086$. Šídák-corrected pairwise comparisons at individual timepoints were not significant (adjusted $p = 0.051$–0.42).

3.5 Qualitative Cellular Uptake: Confocal Microscopy Confirms Perinuclear Curcumin Localisation for Both Formulations

Confocal laser scanning microscopy at 2 h (Fig. 5) showed intact nuclear and cellular morphology in both treatment groups, with no overt morphological signs of cytotoxicity. The 2 h timepoint was selected to capture intracellular distribution during the early accumulation phase. In both Cur-FD- and NP-treated cells, curcumin fluorescence (green) localised predominantly to a band encircling the nucleus, co-localising with the CellTracker Red-defined perinuclear cytoplasmic compartment, rather than distributing diffusely through the cytoplasm. The two formulations differed in the texture of that perinuclear signal: in Cur-FD-treated cells the green signal was more diffuse and reticular, whereas in NP-treated cells the same region resolved into more numerous, discrete vesicular structures, with green signal also extending into fine peripheral projections. Cells exposed to blank (curcumin-free) PLGA NPs showed normal nuclear and CellTracker Red staining (Supplementary material, Fig. S3); as PLGA is not intrinsically fluorescent in the FITC range (Zhukova et al. 2021), the green signal in treated cells is attributed to curcumin. The vesicular texture seen in NP-treated cells is consistent with endocytic uptake and trafficking to the perinuclear endolysosomal compartment (Pu et al. 2016), in line with the enhanced intracellular curcumin accumulation achieved by Cur-PLGA NPs (Section 3.4).

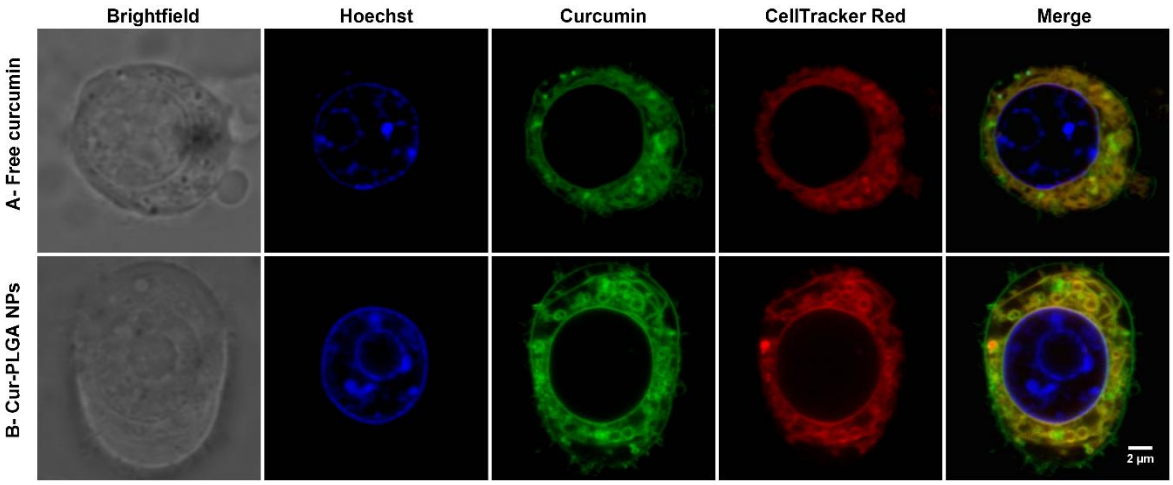


Fig. 5 Intracellular distribution of curcumin in RAW 264.7 macrophages assessed by confocal laser scanning microscopy (CLSM; Olympus FV5000; 100× oil-immersion objective with digital zoom). Cells were treated with 20 µM curcumin-equivalent (A) free curcumin (Cur-FD) or (B) Cur-PLGA NPs for 2 h. Columns show brightfield, Hoechst 33342 (blue, nucleus), curcumin intrinsic fluorescence (green; λex 498 nm, λem 517 nm), CellTracker Red CMTPX (red, cytoplasm) and merged fluorescence channels (additive overlay; no non-linear adjustments). Curcumin localised to a perinuclear band in both groups, with a more vesicular pattern in NP-treated cells, consistent with endolysosomal uptake. Blank PLGA NP controls are shown in Supplementary material, Fig. S3. Representative images are shown. Scale bars, 2 µm.

3.6 Tumour-Derived Paracrine Signals Establish a Non-Classical M1/M2 Transcriptional Profile

Prior to co-culture experiments, the RAW 264.7:4T1 ratio was established by measuring minimum cell diameter across a transwell titration (Supplementary material, Fig. S4). RAW 264.7 cells in monoculture exhibited a mean minimum diameter of 5.83 ± 0.62 µm. Co-culture with 4T1 cells produced an overall reduction in diameter with increasing 4T1 ratio: 5.53 ± 0.87 µm at 1:1, 5.00 ± 0.93 µm at 1:2, 5.08 ± 0.96 µm at 1:3, and 4.72 ± 0.75 µm at 1:4 (approximately 5%, 14%, 13%, and 19% reduction relative to monoculture, respectively; within-experiment statistical comparisons in Supplementary material, Table S3). The 1:2, 1:3, and 1:4 conditions were not substantially different from one another, suggesting the response approaches a plateau by a ratio of 1:2. A 1:3 ratio was selected for subsequent co-culture experiments as a mid-plateau condition. These data derive from a single representative experiment (10 cells × 3 fields per condition, N = 30); independent biological replication is required for definitive conclusions.

To characterise the immunomodulatory effect of tumour-derived signals on macrophage polarisation, RAW 264.7 cells were exposed to 4T1-conditioned medium (4T1-CM) alongside LPS (M1 control) and IL-4 (M2 control), and compared against unstimulated 48 h controls (C48). Following Geisser–Greenhouse correction, the omnibus F-tests did not reach significance for any of the three genes (TNF-α: $F(1.09, 4.38) = 4.49$, $p = 0.094$; ARG1: $F(1.36, 5.44) = 3.14$, $p = 0.130$; *Nfkb1*: $F(1.37, 2.74) = 4.01$, $p = 0.151$), a consequence of the substantial reduction in degrees of freedom that this correction imposes on small-sample repeated-measures designs (ε = 0.36–0.46). Tukey's comparisons, which control family-wise error rate independently of the omnibus test, are therefore reported below.

Assay validity was confirmed by both polarisation controls: LPS upregulated TNF-α relative to C48 (3.11-fold, 95% CI 1.39–6.94; Tukey $p = 0.016$), and IL-4 upregulated ARG1 (14.73-fold, 95% CI 2.82–76.9; $p = 0.009$) (Fig. 6A, B). Against these references, 4T1-CM produced a distinctly non-classical profile. TNF-α was not induced, remaining significantly lower under 4T1-CM than under LPS (0.43-fold relative to LPS, 95% CI 0.23–0.82; $p = 0.020$), while ARG1 showed only a non-significant increase (3.50-fold, 95% CI 0.09–132; $p = 0.556$), indicating that 4T1-CM does not drive classical M1 activation.

Transwell co-culture significantly upregulated ARG1 (mean ΔΔCq −5.09 ± 1.67 (SEM); one-sample $t(4) = 3.06$, $p = 0.038$; geometric mean 34.1-fold, 95% CI 1.4–840; Cohen's $d = 1.37$; $n = 5$) without inducing TNF-α (mean ΔΔCq +0.48 ± 0.57; $p = 0.448$; 0.72-fold, 95% CI 0.24–2.15) (Fig. 6D). Because ARG1 amplified close to the detection threshold in control

samples (Cq > 36 in four of five runs), the magnitude of induction is imprecise, although its direction was consistent in 4 of 5 replicates. Like 4T1-CM, transwell co-culture upregulated ARG1 without inducing TNF-α, indicating that neither model drives canonical M1 activation via this two-marker readout. 4T1-CM was used for all subsequent experiments because it delivers a defined, batch-controlled dose that is independent of tumour cell number and growth rate, giving a more reproducible exposure across the repeated transcriptional, surface-marker and oxidative readouts.

4T1-CM increased *Nfkb1* transcript expression (2.76-fold, 95% CI 2.31–3.30; Tukey p = 0.0003) — but without the concomitant TNF-α induction that characterises canonical M1 activation (Fig. 6C). This dissociation between *Nfkb1* upregulation and its canonical downstream inflammatory output is consistent with a non-classical activation state rather than conventional M1 or M2 polarisation. Consistent with this interpretation, TNF-α and ARG1 ΔΔCq values across treatment conditions correlated positively rather than negatively (ρ = +0.32, 95% CI −0.24 to 0.72; p = 0.243; n = 15, control values excluded as zero by definition), a direction contrary to the reciprocal regulation predicted by the classical M1/M2 model, although not reaching significance. The co-expression of M1 and M2 features characteristic of the hybrid TAM phenotype (Martinez and Gordon 2014; Steenbrugge et al. 2018; Pe et al. 2022) is examined further by the surface marker analysis presented in Section 3.7.

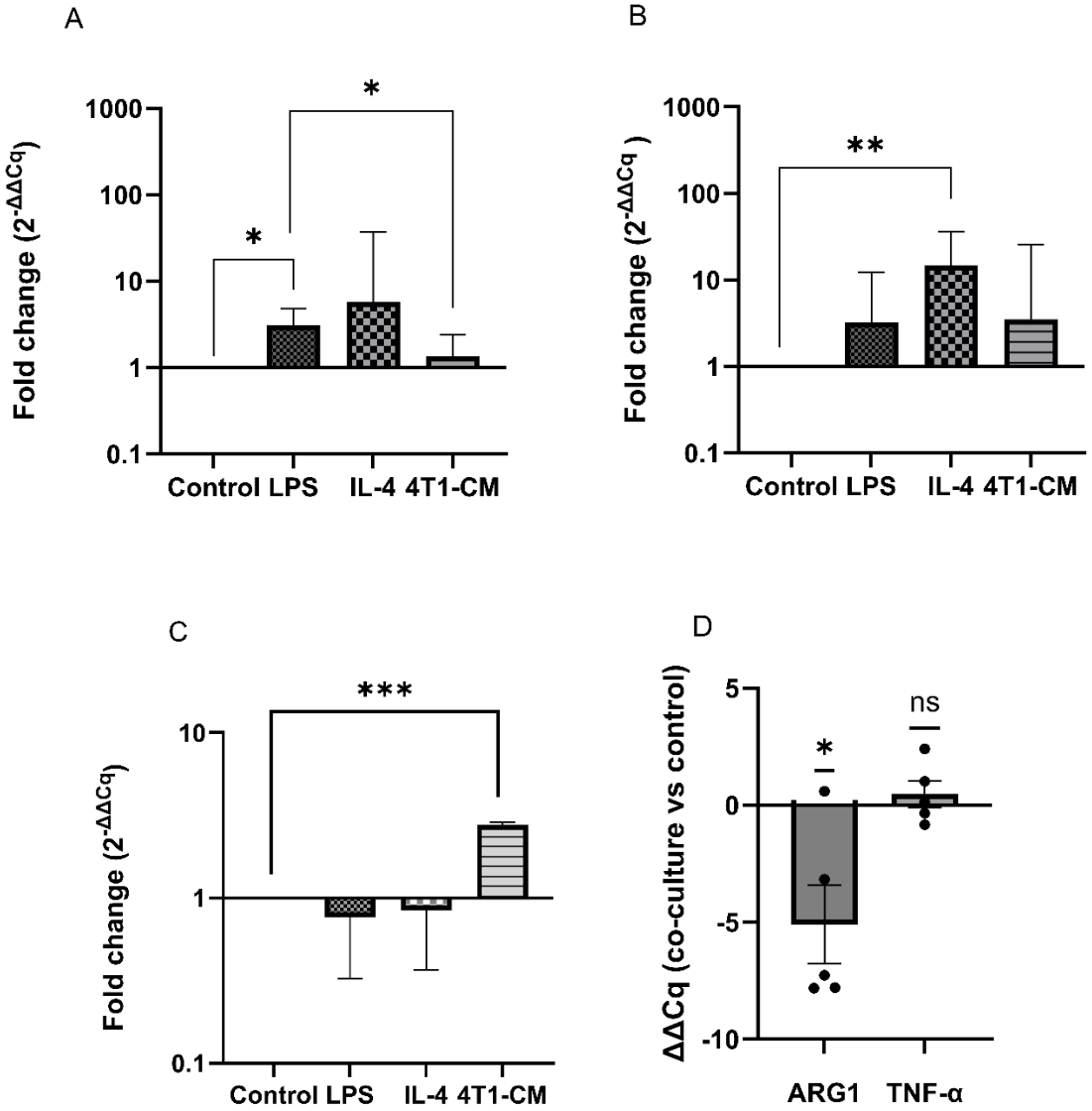


Fig. 6 RT-qPCR analysis of macrophage polarisation markers in RAW 264.7 cells exposed to tumour-derived signals. (A) TNF-α, (B) ARG1 and (C) *Nfkb1* expression following 48 h treatment with LPS (M1 control), IL-4 (M2 control) or 4T1-conditioned medium (4T1-CM), relative to unstimulated 48 h controls (C48; "Control" in the graphs). Bars show geometric mean with geometric SD on a logarithmic y-axis (n = 5 for TNF-α and ARG1; n = 3 for *Nfkb1*). (D) Transwell co-culture of RAW 264.7 cells with 4T1 cells (1:3) for 48 h, analysed separately as a paired within-run comparison against matched controls; bars show mean ΔΔCq ± SEM with individual biological replicates (n = 5), and negative ΔΔCq indicates upregulation. Statistical comparisons were performed on ΔCq values by repeated-measures ANOVA with Geisser–Greenhouse correction followed by Tukey's post-hoc test (A–C), or by one-sample t-test against ΔΔCq = 0 (D). *p < 0.05, **p < 0.01, ***p < 0.001; comparisons without asterisks were not significant. ROUT analysis (Q = 1%) identified no outliers; all values were retained.

3.7 Flow Cytometry Reveals a CD86-Skewed Surface Profile Under 4T1-CM Stimulation

One-way ANOVA of the CD86:CD206 MFI ratio across polarisation conditions (Fig. 7C) was statistically significant ($F(4,10) = 9.75$, $p = 0.0018$). Tukey post-hoc analysis confirmed that 4T1-CM-conditioned macrophages (CD86:CD206 ratio = 1.24) exhibited a significantly higher ratio than all other groups (Control: $p = 0.0048$; LPS: $p = 0.0038$; IL-4: $p = 0.0208$; Co-culture (1:3): $p = 0.0022$), with the ratio higher than the control mean (0.77) in all three biological replicates (1.42, 1.25, 1.05). One-way ANOVA on CD86 MFI alone ($F(4,10) = 3.14$, $p = 0.065$) and CD206 MFI alone ($F(4,10) = 0.59$, $p = 0.68$) did not reach significance across conditions, indicating that the CD86:CD206 ratio, rather than either marker in isolation, distinguishes 4T1-CM stimulation from the other four conditions. Notably, neither reference stimulus shifted its canonical surface marker at 48 h (CD86 MFI: LPS 789 vs. Control 677, Tukey $p = 0.985$; CD206 MFI: IL-4 881 vs. Control 889, $p > 0.999$), so the surface panel was not independently validated by its polarisation controls, and the 4T1-CM ratio is therefore interpreted together with the transcriptional data (Section 3.6).

Co-culture did not reproduce this surface phenotype: its CD86:CD206 ratio (0.71) was the lowest of all five conditions and did not differ significantly from Control, LPS or IL-4 (all $p > 0.5$), despite producing the strongest transcriptional ARG1 induction of any condition (Section 3.6). 4T1-CM, whose CD86-skewed surface profile was concordant with its *Nfkb1* upregulation, was therefore retained as the more tractable model of the hybrid phenotype at the protein level.

Together with the transcriptional profile (Section 3.6), the CD86-skewed surface phenotype under 4T1-CM indicates a hybrid rather than canonical M1 or M2 state characterised by pro-inflammatory signalling (NF-κB, CD86). The immunoregulatory ARG1 arm was significant only under co-culture among tumour-derived conditions, suggesting that 4T1-CM and co-culture capture complementary rather than fully overlapping facets of TAM polarisation.

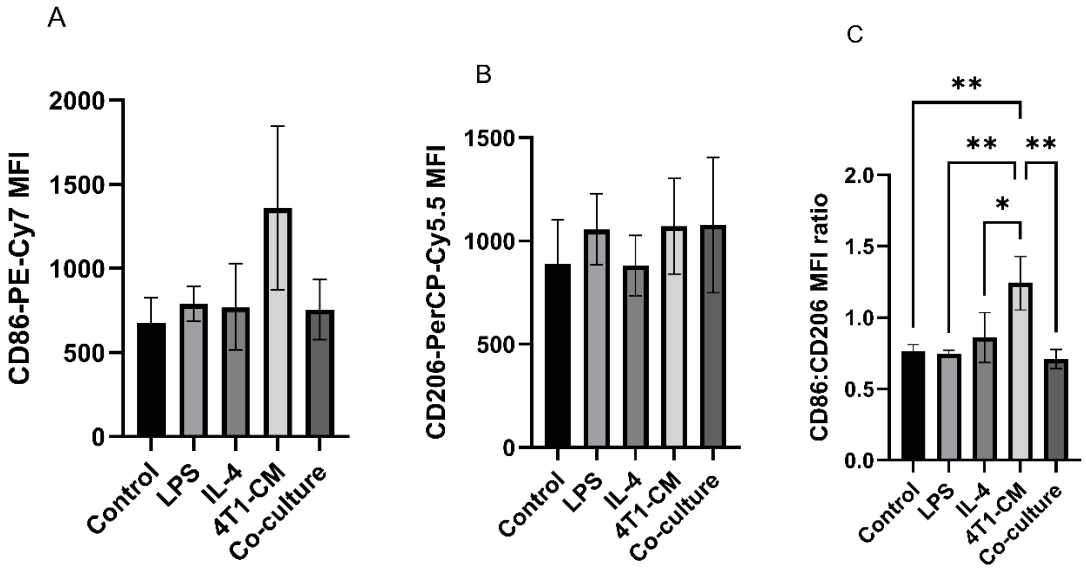


Fig. 7 Flow cytometry surface marker analysis in the polarisation experiment. (A) CD86-PE-Cy7 MFI, (B) CD206-PerCP-Cy5.5 MFI and (C) CD86:CD206 MFI ratio in RAW 264.7 macrophages after 48 h under Control (unstimulated), LPS (100 ng/mL), IL-4 (40 ng/mL), 4T1-CM (1:1 dilution) or Co-culture (transwell, RAW 264.7:4T1 1:3) conditions. Bars show mean ± SD (n = 3 biological replicates). One-way ANOVA: CD86 $F(4,10) = 3.14$, $p = 0.065$; CD206 $F(4,10) = 0.59$, $p = 0.68$; CD86:CD206 ratio $F(4,10) = 9.75$, $p = 0.0018$. Tukey's post-hoc test: in (C), 4T1-CM differed significantly from all other conditions (*$p < 0.05$, **$p < 0.01$); no pairwise comparison reached significance in (A) or (B).

3.8 Biochemical Effector Profile: LPS Drives Oxidative Burst; 4T1-CM Does Not

LPS stimulation elicited significant intracellular ROS elevation (2.70 ± 1.23-fold; $t(4) = 3.082$, $p = 0.037$; one-sample t-test vs. C48 = 1.0; one-way ANOVA $F(2,12) = 4.683$, $p = 0.031$). LPS-induced ROS was significantly greater than in 4T1-CM-conditioned macrophages (Tukey: $p = 0.031$). In contrast, neither IL-4 (1.44-fold, $p = 0.337$) nor 4T1-CM (1.03-fold, $p = 0.787$) significantly differed from the C48 baseline. This represents a biochemical decoupling: *Nfkb1* was elevated (Section 3.6), whereas ROS remained at baseline in 4T1-CM-conditioned macrophages. This pattern is consistent with the hybrid, non-canonical activation state established by the transcriptional (Section 3.6) and surface marker (Section 3.7) data, in which 4T1-CM drives pro-inflammatory signalling without engaging the full canonical M1 effector programme (Fig. 8).

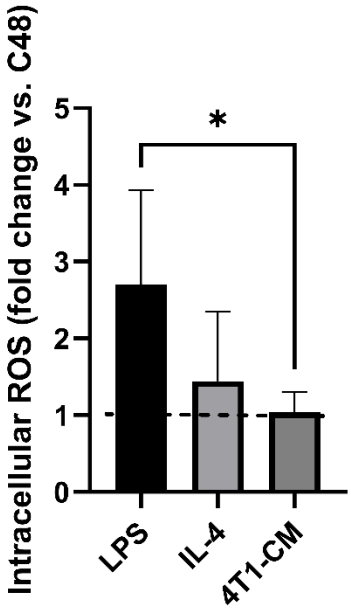


Fig. 8 Intracellular ROS response to macrophage-polarising stimuli. Intracellular ROS (DCFH-DA assay, normalised to protein) after 48 h with LPS (100 ng/mL), IL-4 (40 ng/mL) or 4T1-CM (1:1 dilution), expressed as fold change relative to the unstimulated 48 h control (C48; dashed line = 1.0). Bars show mean ± SD (n = 5 independent experiments). One-way ANOVA, $F(2,12) = 4.68$, $p = 0.031$; Tukey's post-hoc test: *$p < 0.05$, LPS vs. 4T1-CM. One-sample t-tests vs. C48 (not marked on the graph): LPS $p = 0.037$, IL-4 $p = 0.337$, 4T1-CM $p = 0.787$.

3.9 Effect of Macrophage-Conditioned Media on 4T1 Migration

In scratch wound healing assays (n = 8), mean 4T1 wound closure at 24 h followed the order (Fig. 9; replicate-level data in Supplementary material, Table S7): positive control (55.52 ± 24.05%) ≈ M2-CM (52.25 ± 24.03%) > TAM-CM (45.65 ± 21.92%) > negative control (33.02 ± 21.93%) ≈ M1-CM (31.77 ± 20.71%) > 4T1-CM direct (27.23 ± 23.70%). Mean closure with M2-CM approached that of the serum positive control, whereas M1-CM remained close to the serum-restricted negative control (Cohen's d vs. M2-CM = 0.913). TAM-CM produced an intermediate response, positioned between M1-CM and M2-CM and closer to M2-CM in magnitude (d vs. M1-CM = 0.651), consistent with the hybrid, non-

classically-M1 phenotype indicated by the flow cytometry and ROS data above. 4T1-CM applied directly to tumour cells produced the lowest mean closure of all groups, suggesting that residual 4T1-derived factors carried over in TAM-CM do not account for its higher mean closure, which is more likely attributable to macrophage-derived factors.

The overall Kruskal-Wallis test was not significant ($H = 8.80$, $p = 0.117$), and none of the 15 pairwise comparisons reached significance by Dunn's multiple comparisons test, reflecting the high inter-experiment variability inherent to this assay. A post hoc power analysis based on the effect sizes for the key macrophage comparisons ($d = 0.65$ for TAM-CM vs. M1-CM and $d = 0.91$ for M2-CM vs. M1-CM) indicated that substantially larger cohorts (approximately $n = 20–39$ per group, depending on the comparison) would be required to achieve 80% power to detect these differences formally. These findings should therefore be interpreted as a functional trend consistent with the hybrid TAM phenotype established in Sections 3.7–3.8, rather than as a statistically confirmed hierarchy, and warrant validation in a higher-powered cohort.

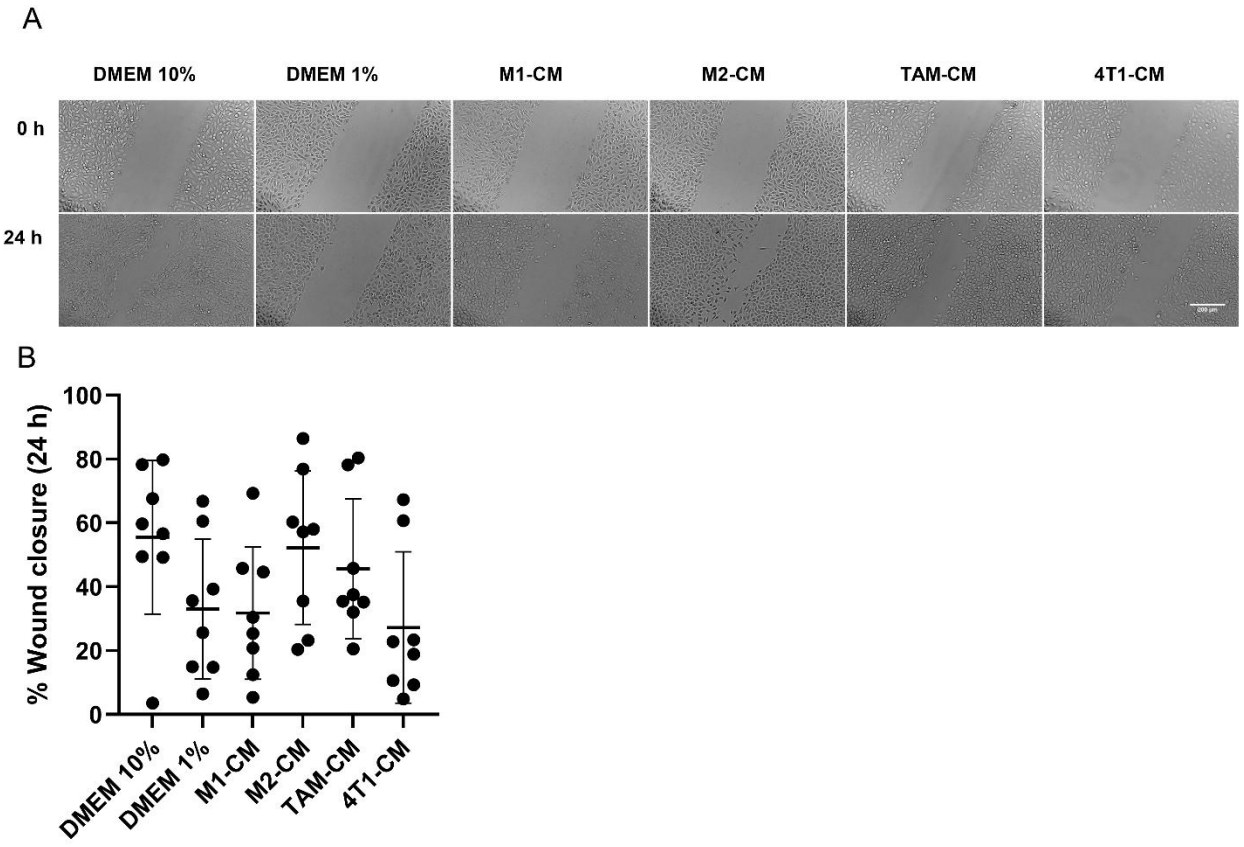


Fig. 9 Effect of macrophage-conditioned media on 4T1 cell migration. (A) Representative phase-contrast images (10×) of 4T1 scratch wounds at 0 h and 24 h after treatment with DMEM 10% (positive control), DMEM 1% (negative control), M1-CM, M2-CM, TAM-CM or 4T1-CM, from one representative experiment (replicate T3, Supplementary material, Table S7). Images were converted to greyscale, and a linear contrast adjustment was applied identically to all panels. Scale bar, 200 µm (applies to all panels). (B) Percentage wound closure at 24 h, calculated as $[(W_0 - W_{24})/W_0] \times 100$, where W is the mean scratch width from three measurements per field ($n = 8$ independent experiments per group). Horizontal lines

show the mean ± SD, with individual values shown as dots. Group means followed the order DMEM 10% ≈ M2-CM > TAM-CM > DMEM 1% ≈ M1-CM > 4T1-CM, but differences were not statistically significant (Kruskal–Wallis test, H = 8.80, p = 0.117; Dunn's multiple comparisons test, all pairwise comparisons p > 0.05).

3.10 Cur-PLGA Nanoparticles Drive Transcriptional Repolarisation of 4T1-CM-Educated Macrophages, with Concordant Surface and Biochemical Trends

3.10.1 Transcriptional Reprogramming: TNF-α, ARG1, and Nfkb1

Before assessing repolarisation, the sequential 48 h → 96 h design was validated by confirming that untreated RAW 264.7 cells show minimal target gene drift between the 48 h and 96 h timepoints (paired t-tests). TNF-α and ARG1 showed no significant change between 48 h and 96 h (p=0.590 and p=0.488, respectively); *Nfkb1* showed a small but statistically significant increase (1.23-fold, p=0.019), substantially smaller than the treatment-induced changes reported below (4.7–17.2-fold), indicating that time-in-culture alone cannot account for the repolarisation effects observed. Agreement between paired measurements across this window was high for ARG1 (ICC(2,1) = 0.971), moderate for *Nfkb1* (ICC(2,1) = 0.611) and lower for TNF-α (ICC(2,1) = 0.335), reflecting greater within-pair scatter in TNF-α ΔCq rather than a systematic time-dependent shift, as confirmed by its non-significant paired t-test above (Supplementary material, Fig. S6 and Table S8).

Following 4T1-CM conditioning for 48 h, macrophages were treated with 0.25 μM Cur-FD or Cur-PLGA NPs for a further 48 h. Cur-PLGA NPs significantly upregulated TNF-α relative to the 4T1-CM-primed reference (5.8-fold, 95% CI 3.7–9.0; Tukey p = 0.003), whereas the increase with Cur-FD (5.5-fold, 95% CI 0.6–51.9) did not reach significance (p = 0.084), and the two formulations did not differ (p = 0.984) (repeated-measures ANOVA with Geisser–Greenhouse correction, F(1.01, 2.02) = 24.00, p = 0.038). ARG1 showed a non-significant suppression trend with both Cur-FD (~80%; p = 0.153) and Cur-PLGA NPs (~67%; p = 0.230) (F(1.48, 2.96) = 7.61, p = 0.070), reflecting high inter-replicate variability in ARG1 ΔCq at n = 3. Calculated as in Section 3.6 (reference condition excluded), the TNF-α/ARG1 Spearman correlation remained weakly positive and non-significant after repolarisation (ρ = +0.37, 95% CI −0.65 to 0.91, p = 0.50, n = 6), so no change in TNF-α/ARG1 co-regulation could be resolved at this sample size (Fig. 10).

Cur-PLGA NPs increased NF-κB transcript expression 17.2-fold relative to the 4T1-CM-primed reference (Tukey 95% CI 12.2–24.3; p < 0.001), with consistent paired fold changes across the three biological replicates (Supplementary material, Table S4). Cur-FD showed a directional but non-significant trend (~4.7-fold; p = 0.137), consistent with lower intracellular delivery relative to Cur-PLGA NPs (Section 3.4); the difference between formulations was not significant (p = 0.166). Because 4T1-CM alone had already increased *Nfkb1* expression without inducing TNF-α (Section 3.6), the concurrent TNF-α increase suggests that Cur-PLGA NPs coupled *Nfkb1* to its pro-inflammatory output rather than only increasing its expression. Tumour-derived IL-10 and TGF-β1 can restrain this downstream output in tumour-conditioned macrophages, and curcumin may relieve the restraint through STAT3/STAT6/PI3K inhibition (Hagemann et al. 2008; Connelly et al. 2011; Jiang et al. 2022; Deswal et al. 2024). This differs from its anti-inflammatory role in LPS-stimulated M1 cells (Zhao et al. 2015) (Fig. 10C).

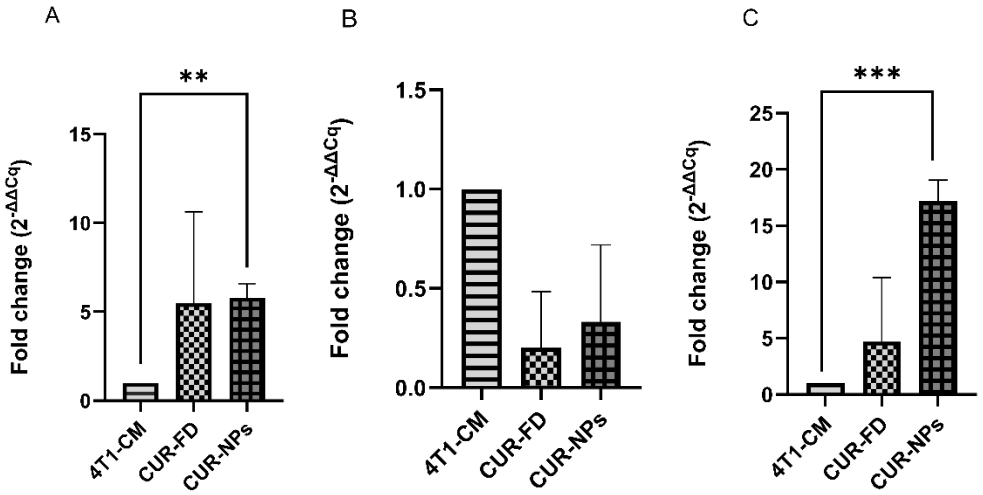


Fig. 10 Transcriptional repolarisation of 4T1-CM-primed macrophages by Cur-PLGA NPs and free curcumin. RAW 264.7 macrophages were conditioned with 4T1-CM for 48 h, then treated with 0.25 μM Cur-FD or Cur-PLGA NPs for a further 48 h. Gene expression (RT-qPCR, 2^−ΔΔCq) is shown relative to the 4T1-CM-primed reference (= 1.0). (A) TNF-α increased with Cur-PLGA NPs (5.8-fold, p = 0.003) and non-significantly with Cur-FD (5.5-fold, p = 0.084). (B) ARG1 decreased non-significantly with Cur-FD (~80%, p = 0.153) and Cur-PLGA NPs (~67%, p = 0.230). (C) *Nfkb1* increased with Cur-PLGA NPs (17.2-fold, p < 0.001) but not significantly with Cur-FD (4.7-fold, p = 0.137). Bars show geometric mean with geometric SD (n = 3 biological replicates). Statistics were performed on ΔCq values by repeated-measures ANOVA with Geisser–Greenhouse correction and Tukey's post-hoc test; **p < 0.01, ***p < 0.001 vs. 4T1-CM; comparisons without asterisks were not significant.

3.10.2 Surface Marker Phenotype: CD86:CD206 Ratio

Surface phenotype was assessed at the same 96 h endpoint as the transcriptional analysis, relative to a matched 4T1-CM-primed, vehicle-treated 96 h control (C96; distinct from the qPCR repolarisation reference, which reuses the 48 h 4T1-CM timepoint; Section 3.10.1). Both formulations numerically increased CD86 MFI (C96: 1721 ± 369; Cur-FD: 2982 ± 1677, ~1.7-fold; Cur-PLGA NP: 2884 ± 1667, ~1.7-fold), whereas CD206 MFI remained essentially unchanged (C96: 1271 ± 154; Cur-FD: 1326 ± 392, ~1.0-fold; Cur-PLGA NP: 1236 ± 299, ~1.0-fold). Neither marker differed significantly by one-way ANOVA (CD86: $F(2,6) = 0.774$, $p = 0.502$; CD206: $F(2,6) = 0.070$, $p = 0.933$), reflecting the high inter-replicate variance of MFI measurements at this sample size.

Consequently, the CD86:CD206 MFI ratio, a composite indicator of M1/M2 phenotypic balance was increased from 1.36 ± 0.29 in the 4T1-CM-primed, vehicle-treated 96 h reference (C96; distinct from the 48 h polarisation-panel 4T1-CM ratio of 1.24 in Section 3.7, reflecting the additional 48 h of tumour-conditioned culture) to 2.17 ± 0.63 with Cur-FD and 2.23 ± 0.74 with Cur-PLGA NPs (~1.6-fold for both formulations). This shift corresponded to large effect sizes (Cohen's d = 1.65 for Cur-FD, 1.54 for Cur-PLGA NP) but did not reach statistical significance at the current sample size (one-way ANOVA $F(2,6) = 2.053$, $p = 0.209$; Tukey's post-hoc: C96 vs Cur-FD $p = 0.284$, C96 vs Cur-PLGA NP $p = 0.244$, Cur-FD vs Cur-PLGA NP $p = 0.992$). Post-hoc power analysis indicated that n = 7–8 per group would be required to detect effects of this magnitude at 80% power. The n = 3 design is therefore underpowered for this comparison, and the lack of significance should not be taken as evidence of no effect.

The ratio shift was driven by CD86 upregulation rather than CD206 loss, indicating a partial M1 skew of the surface phenotype within this 48 h window that is directionally consistent with, but less complete than, the transcriptional reprogramming (Section 3.10.1; Fig. 11).

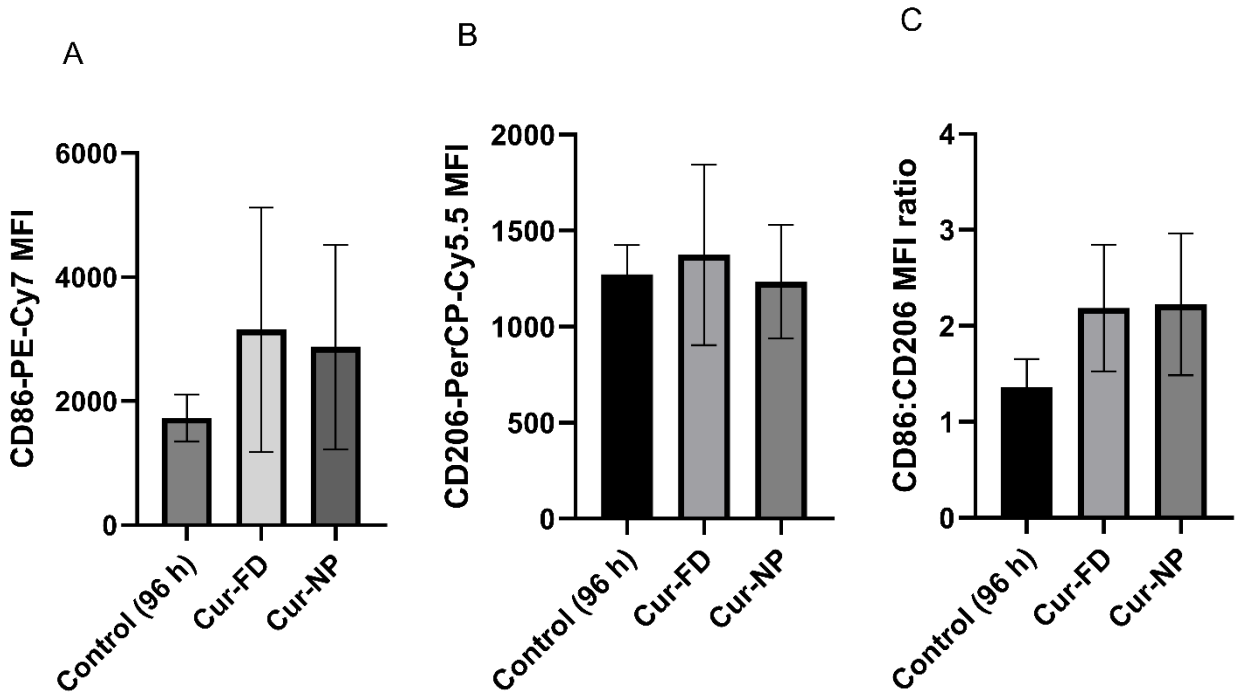


Fig. 11 Effect of Cur-PLGA nanoparticles and free curcumin on the surface phenotype of 4T1-CM-primed macrophages. RAW 264.7 macrophages were conditioned with 4T1-CM for 48 h, then treated with 0.25 μM Cur-FD or Cur-PLGA NPs for a further 48 h; the Control (96 h) reference received vehicle instead of curcumin for the second 48 h. (A) CD86-PE-Cy7 MFI increased non-significantly with Cur-FD (~1.7-fold) and Cur-PLGA NPs (~1.7-fold) relative to Control (96 h) ($F(2,6) = 0.77$, $p = 0.502$). (B) CD206-PerCP-Cy5.5 MFI was unchanged ($F(2,6) = 0.07$, $p = 0.933$). (C) The CD86:CD206 MFI ratio increased ~1.6-fold with both treatments ($F(2,6) = 2.05$, $p = 0.209$). Bars show mean ± SD (n = 3 biological replicates). One-way ANOVA with Tukey's post-hoc test; no pairwise comparisons were significant.

3.10.3 Oxidative Burden: ROS Trend

Intracellular ROS was measured by DCFH-DA fluorescence following the same sequential design (48 h 4T1-CM priming, then 48 h Cur-FD or Cur-PLGA NP treatment), expressed as fold-change relative to a matched 4T1-CM-primed, vehicle-treated 96 h reference (C96, normalised to 1.0). Both formulations produced a modest, non-significant increase in ROS relative to the 4T1-CM-primed baseline: Cur-FD averaged 1.40 ± 0.87-fold (one-sample t-test vs. baseline = 1, $p = 0.508$) and Cur-PLGA NPs averaged 1.36 ± 0.67-fold ($p = 0.449$) (Fig. 12), with no significant difference between the two formulations (Welch's t-test, $t = 0.066$, $df = 3.75$, $p = 0.951$; Cohen's $d = 0.05$). Post-hoc power analysis indicated that ≥29–39 replicates per group would be required to detect effects of this magnitude at 80% power, so these comparisons are substantially underpowered and cannot exclude a modest ROS response. The high inter-replicate variance in both groups (driven by one high-responding replicate reaching >2-fold in each arm) suggests possible passage- or batch-dependent heterogeneity in oxidative response, which a larger, more tightly controlled cohort would be needed to resolve.

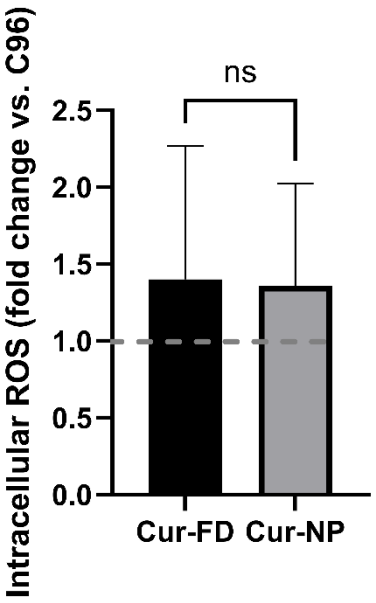


Fig. 12 Cur-PLGA nanoparticles and free curcumin do not significantly alter intracellular ROS in 4T1-CM-primed macrophages. RAW 264.7 macrophages were conditioned with 4T1-CM for 48 h, then treated with 0.25 μM Cur-FD or Cur-PLGA NPs for a further 48 h; the Control (96 h, C96) reference received vehicle instead of curcumin for the second 48 h. Intracellular ROS (DCFH-DA assay, normalised to protein) is expressed as fold change relative to C96 (dashed line = 1.0). Both formulations produced a modest, non-significant increase (Cur-FD 1.40-fold, $p = 0.508$; Cur-PLGA NPs 1.36-fold, $p = 0.449$; one-sample t-tests vs. 1.0), with no difference between formulations (Welch's t-test, $p = 0.951$). Bars show mean ± SD (n = 3 independent experiments).

4. Discussion

4.1 Formulation, pH-Responsive Release and Macrophage Uptake

At 240.5 nm (PDI 0.076), the nanoparticles lie within the 200–500 nm range preferentially internalised by phagocytic cells via clathrin-mediated and macropinocytic pathways (Astete and Sabliov 2006; Makadia and Siegel 2011; Paladugulu et

al. 2025), and the drug loading (279.91 ± 33.32 μg curcumin/mg NP) is consistent with partitioning of lipophilic curcumin (log P ~3.0) into the hydrophobic PLGA matrix (Yallapu et al. 2012).

Cumulative release at 30 days increased from 36% at pH 7.4 to 38% at pH 6.4 and 45% at pH 4.5, consistent with faster PLGA ester hydrolysis in the acidic macrophage endolysosome (pH 4.5–5.0) (Galloway et al. 1983). Because release was quantified as intact curcumin, pH-dependent degradation of released drug may also contribute to the pH differences in measured release. In earlier work from our laboratory, free curcumin incubated in PBS at 37 °C retained approximately 70% of its initial content at pH 4.5 but only about 51% at pH 7.4 after 96 h, consistent with the known pH dependence of curcumin degradation (Wang et al. 1997; Praveena and Guru 2021). Degradation is unlikely to dominate the measured profiles, however: the 2 h burst did not differ between pH values, the profiles diverged only after 12–24 h, and release at pH 7.4 remained at a stable plateau from 24 h to 30 days rather than declining. The Tween 80 in the release medium likely limited this degradation, as micellar solubilisation can slow curcumin degradation compared with plain buffer (Naksuriya et al. 2016). The higher release at acidic pH therefore probably reflects both faster release and greater stability of curcumin under acidic conditions. The ~19% burst within 2 h, typical of curcumin–PLGA systems (Roshan et al. 2024), likely reflects surface-associated drug, whereas the ~55–64% not released by 30 days is consistent with retention in the compact matrix, although residual drug in the NP pellet was not quantified. Retention at physiological pH combined with preferential release under acidic conditions favours delivery after macrophage uptake rather than premature extracellular loss. The uptake data support this: NP-derived intracellular curcumin rose sharply by 4 h and remained elevated to 12 h (42 versus 18 nmol/mg protein for Cur-FD), and NP-treated cells showed a finely vesicular perinuclear signal, the expected signature of endocytic trafficking to perinuclear lysosomes, whereas Cur-FD gave a diffuse, reticular pattern consistent with passive partitioning into lipid compartments (Galloway et al. 1983; Yallapu et al. 2012). This difference in intracellular exposure provides a plausible basis for the stronger NP responses during repolarisation.

4.2 The 4T1 TNBC Secretome Establishes a Hybrid TAM-like Phenotype

4T1-CM-stimulated macrophages showed a hybrid phenotype across several readouts: reproducible *Nfkb1* upregulation (2.76-fold, $p = 0.0003$) without TNF-α induction, a CD86:CD206 ratio higher than control (1.24 vs 0.77; the highest of all polarisation conditions), baseline ROS (1.03-fold, $p = 0.787$) and a positive but non-significant TNF-α/ARG1 correlation ($\rho = +0.32$, $p = 0.243$), a direction opposite to the reciprocal regulation predicted by the classical M1/M2 model (Martinez and Gordon 2014; Pe et al. 2022). Tumour-derived factors can activate NF-κB through CSF-1R and IL-6Rα, sustain ARG1 through TGF-β1/Smad signalling and suppress oxidative effector function through IL-10 (Martinez and Gordon 2014; Steenbrugge et al. 2018; Pe et al. 2022), although these factors were not measured in 4T1-CM here. The intermediate effect of TAM-CM on 4T1 wound closure (45.65%, between M1-CM at 31.77% and M2-CM at 52.25%; not significant) and the reduced minimum diameter of co-cultured macrophages, which may reflect elongation linked to immune regulation (McWhorter et al. 2013; Kizhakkanoodan et al. 2026), are consistent with this interpretation but remain preliminary. Both conditioned medium and transwell co-culture are used to generate tumour-educated macrophages (Jiang et al. 2022), yet here they diverged: co-culture gave the strongest ARG1 induction, whereas 4T1-CM gave significant *Nfkb1* upregulation and the only CD86-skewed surface profile. Several differences plausibly account for this. Conditioned medium delivers a fixed, one-way dose of factors accumulated over 48 h, whereas co-culture provides continuous, bidirectional signalling. Short-lived mediators such as prostaglandin E2 and extracellular vesicles decay in collected medium but are continuously replenished in co-culture. Co-culture also imposes metabolic competition: tumour glycolysis depletes glucose and accumulates lactate, itself a potent inducer of arginase-1 (Colegio et al. 2014), which plausibly explains the stronger ARG1 response. The exposures are also not dose-matched, as a 1:1 medium dilution and a 1:3 cell ratio cannot be equated. Co-culture is therefore the closer structural analogue of the tumour microenvironment, whereas conditioned medium delivers a defined, batch-controlled dose independent of tumour cell number and growth rate. Conditioned medium was used for the repolarisation experiments on that basis, and because its hybrid profile resembles the mixed M1/M2 phenotype reported for TNBC tumour-associated macrophages (Pe et al. 2022). Neither reproduces the stromal, hypoxic and immune context of tumour-associated macrophages in vivo; benchmarking against macrophages sorted from 4T1 tumours would be needed to establish which is closer.

4.3 Cur-PLGA NPs Repolarise Tumour-Educated Macrophages Predominantly at the Transcriptional Level

Against a matched 4T1-CM-primed reference, Cur-PLGA NPs significantly increased TNF-α (5.8-fold, $p = 0.003$) and *Nfkb1* transcript expression (17.2-fold, $p < 0.001$), whereas equimolar Cur-FD gave smaller, non-significant increases (5.5-fold, $p = 0.084$, and 4.7-fold, $p = 0.137$, respectively). The difference between formulations for *Nfkb1* was not itself significant ($p = 0.166$), but the larger and more consistent NP response agrees with their 2.3–4.4-fold greater intracellular curcumin accumulation from 4 h onwards. Because 4T1-CM alone had already increased *Nfkb1* expression without

inducing TNF-α (Section 3.6), the key change after curcumin treatment, significant only with Cur-PLGA NPs, was that a further *Nfkb1* increase was accompanied by TNF-α induction.

Three considerations bear on this difference from LPS-activated macrophages. First, the readouts differ: curcumin's reported anti-inflammatory action in LPS-activated macrophages is defined mainly by reduced pathway activity, such as IκBα degradation and p65 phosphorylation and nuclear translocation (Zhao et al. 2015), whereas the present study measured *Nfkb1* transcript abundance. *Nfkb1* encodes p105/p50, is itself an NF-κB-responsive gene, and contributes both to transactivating p65/p50 heterodimers and to repressive p50/p50 homodimers, so an increase in its transcript does not by itself establish the direction of pathway output. Second, the baseline states differ: LPS produces near-maximal pathway activation, in which a modulator can mainly reduce signalling, whereas the tumour-educated macrophages here were in a partially restrained state, with *Nfkb1* elevated but TNF-α not induced (Section 3.6). Third, the consequences of NF-κB modulation in macrophages are context-dependent rather than uniformly directional: NF-κB signalling has been reported to maintain the immunosuppressive tumour-associated macrophage phenotype, with IKKβ inhibition switching these cells to an IL-12^high, arginase-1^low state (Hagemann et al. 2008), whereas NF-κB activation within macrophages has also been reported to produce an anti-tumour phenotype (Connelly et al. 2011). In the present data, the arginase-1 decrease is consistent with a shift away from the immunoregulatory arm, whereas the concurrent *Nfkb1* and TNF-α increases cannot by themselves distinguish pro-inflammatory reprogramming from intensified tumour-type activation. Because repolarisation fold changes are expressed relative to the primed state, they are not directly comparable with the initial 4T1-CM-induced increase (2.76-fold vs. C48). Resolving the functional direction would require IL-12 and MHC II readouts alongside protein-level assessment of pathway activity, such as phospho-IκBα and p65 nuclear translocation.

The remaining readouts moved in the same direction but less completely. ARG1 fell by ~67% and the CD86:CD206 ratio rose from 1.36 to 2.23, driven by CD86 rather than CD206 loss, but neither change was significant at n = 3, and intracellular ROS rose only slightly (1.36-fold with NPs), mirroring the *Nfkb1*–ROS decoupling seen during 4T1-CM polarisation. The 48 h treatment window may be too short for a complete surface transition, as mannose receptor activity responds to modulating signals over several days (Mokoena and Gordon 1985). Curcumin nanoformulations have similarly shifted macrophage balance in TNBC (Shiri et al. 2015) and in other tumour models (Lu et al. 2016), and curcumin suppresses NF-κB-linked metastasis in breast cancer (Aggarwal et al. 2005). Pharmacologically, these data show that nanoencapsulation delivers curcumin to macrophages at a sub-cytotoxic concentration of 0.25 μM, 20–80-fold below the 5–20 μM previously used to reprogramme tumour-educated macrophages (Jiang et al. 2022), and produces reproducible transcriptional reprogramming of tumour-educated macrophages, supporting its development as an adjuvant to immunotherapy or chemotherapy in TNBC.

4.4 Limitations and Future Directions

RAW 264.7 cells have constitutively active NF-κB and more limited M2 plasticity than primary bone marrow-derived macrophages (BMDMs) (Yunna et al. 2020; Ding et al. 2025), and the two education models were compared in vitro only, so which better reproduces tumour-associated macrophages in vivo is unresolved. Repolarisation was tested at a single sub-cytotoxic concentration (0.25 μM), and the readouts were principally transcriptional. IL-12 and MHC II were not measured, and pathway activity was not assessed at protein level, so the functional direction of the *Nfkb1* increase remains unestablished. The surface-marker and ROS readouts were exploratory and underpowered (7–8 and ≥29 replicates per group required). The morphometry derives from a single experiment, and the wound-healing assay (n = 8) could not separate migration from proliferation. The migration assay was omitted from the repolarisation arm because residual curcumin can inhibit tumour-cell migration directly (Wang et al. 2020).

Future work should therefore add IL-12 and MHC II readouts with protein-level measures of pathway activity and compare LPS-activated and tumour-educated macrophages in parallel to test context dependence directly. Whether curcumin's inhibition of STAT3, STAT6 and PI3K signalling (Jiang et al. 2022; Deswal et al. 2024) contributes to the responses observed here also remains to be tested.

5. Conclusions

Cur-PLGA NPs showed pH-dependent curcumin release, lowest at physiological pH and highest at endolysosomal pH 4.5 (Astete and Sabliov 2006; Makadia and Siegel 2011; Paladugulu et al. 2025), and from 4 h onwards delivered 2.3–4.4-fold more intracellular curcumin to macrophages than free curcumin. 4T1-CM induced a hybrid rather than classical M1 or M2 macrophage phenotype (Martinez and Gordon 2014; Pe et al. 2022), and Cur-PLGA NPs produced transcriptional changes in these tumour-educated macrophages, with significant *Nfkb1* and TNF-α upregulation, directional ARG1 suppression and a CD86:CD206 increase, consistent with attenuation of the immunosuppressive signature. These findings support Cur-

PLGA NPs as a candidate macrophage-directed platform for TNBC, pending confirmation of the functional direction and evaluation in primary macrophages and in vivo.

Acknowledgements

The authors thank the National Centre for Cell Science (NCCS, Pune, India) for providing the RAW 264.7 cell line and Dr. K. Nanda Kumar (Manipal College of Pharmaceutical Sciences, MAHE) for the gift of the 4T1 cell line. Technical support from the Manipal Academy of Higher Education, is gratefully acknowledged. The authors also thank the Department of Pathology, Kasturba Medical College (KMC), Manipal; the Manipal Centre for Biotherapeutics Research (MCBR), Manipal; and the Department of Ageing Research, MSLS, Manipal, for their support. We further acknowledge the applications and technical support team (Dr. KN Ganesh & Shivaprasad PS) at Olympus Corporation for assistance with confocal laser scanning microscopy, and the various reagent, chemical, and labware suppliers listed in Section 2.1 for their materials support. Keerthana Suresh Kizhakkanoodan gratefully acknowledges the Manipal Academy of Higher Education (MAHE), Manipal, for the Dr. TMA Pai Fellowship. The authors used ChatGPT/Claude solely for language editing to improve grammar, clarity and readability.

Statements and Declarations

Funding

This work was supported by the Manipal Academy of Higher Education (MAHE) Research Fund, Manipal, India.

Competing interests

The authors have no relevant financial or non-financial interests to disclose.

Author contributions

Keerthana Suresh Kizhakkanoodan: Conceptualization, Methodology, Investigation, Formal analysis, Writing – original draft. Sindhura Lakshmi Koulmane Laxminarayana: Investigation, Resources, Writing – review & editing. Deepali Vengala: Investigation, Writing – review & editing. Nithya Swarandika Sappani: Investigation, Writing – review & editing. Kanive Parashiva Guruprasad: Writing – review & editing. Bharath Raja Guru: Conceptualization, Supervision, Project administration, Funding acquisition, Writing – review & editing.

Ethics approval

This study did not involve human participants, human data, or live animals. RAW 264.7 (murine macrophage) and 4T1 (murine mammary carcinoma) cells used in this work are established cell lines, obtained from the National Centre for Cell Science (NCCS, Pune, India) and gifted by Dr. K. Nanda Kumar (Manipal College of Pharmaceutical Sciences, MAHE), respectively; no primary animal tissue was harvested for this study.

Consent to participate

Not applicable.

Consent for publication

Not applicable.

Data availability

The raw data supporting the conclusions of this article will be made available by the corresponding author on request.

References

Aggarwal BB, Harikumar KB (2009) Potential therapeutic effects of curcumin, the anti-inflammatory agent, against neurodegenerative, cardiovascular, pulmonary, metabolic, autoimmune and neoplastic diseases. Int J Biochem Cell Biol 41:40–59. https://doi.org/10.1016/j.biocel.2008.06.010

Aggarwal BB, Shishodia S, Takada Y, et al (2005) Curcumin suppresses the paclitaxel-induced nuclear factor-kappaB pathway in breast cancer cells and inhibits lung metastasis of human breast cancer in nude mice. Clin Cancer Res 11:7490–8. https://doi.org/10.1158/1078-0432.CCR-05-1192

Anand P, Kunnumakkara AB, Newman RA, Aggarwal BB (2007) Bioavailability of curcumin: problems and promises. Mol Pharm 4:807–18. https://doi.org/10.1021/mp700113r

Astete CE, Sabliov CM (2006) Synthesis and characterization of PLGA nanoparticles. J Biomater Sci Polym Ed 17:247–89. https://doi.org/10.1163/156856206775997322

Biswas SK, Mantovani A (2010) Macrophage plasticity and interaction with lymphocyte subsets: cancer as a paradigm. Nat Immunol 11:889–96. https://doi.org/10.1038/ni.1937

Bray F, Laversanne M, Sung H, et al (2024) Global cancer statistics 2022: GLOBOCAN estimates of incidence and mortality worldwide for 36 cancers in 185 countries. CA Cancer J Clin 74:229–263. https://doi.org/10.3322/caac.21834

Bustin SA, Benes V, Garson JA, et al (2009) The MIQE Guidelines: Minimum Information for Publication of Quantitative Real-Time PCR Experiments. Clin Chem 55:611–622. https://doi.org/10.1373/clinchem.2008.112797

Cassetta L, Pollard JW (2023) A timeline of tumour-associated macrophage biology. Nat Rev Cancer 23:238–257. https://doi.org/10.1038/s41568-022-00547-1

Colegio OR, Chu N-Q, Szabo AL, et al (2014) Functional polarization of tumour-associated macrophages by tumour-derived lactic acid. Nature 513:559–63. https://doi.org/10.1038/nature13490

Connelly L, Barham W, Onishko HM, et al (2011) NF-kappaB activation within macrophages leads to an anti-tumor phenotype in a mammary tumor lung metastasis model. Breast Cancer Research 13:. https://doi.org/10.1186/bcr2935

Deswal B, Bagchi U, Kapoor S (2024) Curcumin Suppresses M2 Macrophage-derived Paclitaxel Chemoresistance through Inhibition of PI3K-AKT/STAT3 Signaling. Anticancer Agents Med Chem 24:146–156. https://doi.org/10.2174/0118715206275259231105184959

Ding T, Du Y, Yang B, et al (2025) Comprehensive review of macrophage models: primary cells and immortalized lines across species. Front Immunol 16:1640935. https://doi.org/10.3389/fimmu.2025.1640935

Galloway CJ, Dean GE, Marsh M, et al (1983) Acidification of macrophage and fibroblast endocytic vesicles in vitro. Proc Natl Acad Sci U S A 80:3334–8. https://doi.org/10.1073/pnas.80.11.3334

Hagemann T, Lawrence T, McNeish I, et al (2008) "Re-educating" tumor-associated macrophages by targeting NF-kappaB. J Exp Med 205:1261–8. https://doi.org/10.1084/jem.20080108

Italiani P, Boraschi D (2014) From Monocytes to M1/M2 Macrophages: Phenotypical vs. Functional Differentiation. Front Immunol 5:514. https://doi.org/10.3389/fimmu.2014.00514

Jiang M, Qi Y, Huang W, et al (2022) Curcumin Reprograms TAMs from a Protumor Phenotype towards an Antitumor Phenotype via Inhibiting MAO-A/STAT6 Pathway. Cells 11:. https://doi.org/10.3390/cells11213473

Kizhakkanoodan KS, Inigo VJ, Koulmane Laxminarayana SL, et al (2026) Morpho-functional plasticity of tumour-associated macrophages: linking cell shape, ultrastructure, and immune regulation in cancer. Clin Exp Med 26:. https://doi.org/10.1007/s10238-026-02190-8

Kizhakkanoodan KS, Rallapalli Y, Praveena J, et al (2023) Cancer nanomedicine: emergence, expansion, and expectations. SN Appl Sci 5:385. https://doi.org/10.1007/s42452-023-05593-4

Lawrence T, Natoli G (2011) Transcriptional regulation of macrophage polarization: enabling diversity with identity. Nat Rev Immunol 11:750–61. https://doi.org/10.1038/nri3088

Liu T, Zhang L, Joo D, Sun S-C (2017) NF-κB signaling in inflammation. Signal Transduct Target Ther 2:17023-. https://doi.org/10.1038/sigtrans.2017.23

Livak KJ, Schmittgen TD (2001) Analysis of relative gene expression data using real-time quantitative PCR and the 2(-Delta Delta C(T)) Method. Methods 25:402–8. https://doi.org/10.1006/meth.2001.1262

Lu Y, Miao L, Wang Y, et al (2016) Curcumin Micelles Remodel Tumor Microenvironment and Enhance Vaccine Activity in an Advanced Melanoma Model. Mol Ther 24:364–374. https://doi.org/10.1038/mt.2015.165

Makadia HK, Siegel SJ (2011) Poly Lactic-co-Glycolic Acid (PLGA) as Biodegradable Controlled Drug Delivery Carrier. Polymers (Basel) 3:1377–1397. https://doi.org/10.3390/polym3031377

Martinez FO, Gordon S (2014) The M1 and M2 paradigm of macrophage activation: time for reassessment. F1000Prime Rep 6:13. https://doi.org/10.12703/P6-13

McWhorter FY, Wang T, Nguyen P, et al (2013) Modulation of macrophage phenotype by cell shape. Proc Natl Acad Sci U S A 110:17253–8. https://doi.org/10.1073/pnas.1308887110
Menon VP, Sudheer AR (2007) Antioxidant and anti-inflammatory properties of curcumin. Adv Exp Med Biol 595:105–25. https://doi.org/10.1007/978-0-387-46401-5_3
Mokoena T, Gordon S (1985) Human macrophage activation. Modulation of mannosyl, fucosyl receptor activity in vitro by lymphokines, gamma and alpha interferons, and dexamethasone. J Clin Invest 75:624–31. https://doi.org/10.1172/JCI111740
Mosser DM, Edwards JP (2008) Exploring the full spectrum of macrophage activation. Nat Rev Immunol 8:958–69. https://doi.org/10.1038/nri2448
Murdoch C, Muthana M, Coffelt SB, Lewis CE (2008) The role of myeloid cells in the promotion of tumour angiogenesis. Nat Rev Cancer 8:618–31. https://doi.org/10.1038/nrc2444
Murray PJ, Allen JE, Biswas SK, et al (2014) Macrophage activation and polarization: nomenclature and experimental guidelines. Immunity 41:14–20. https://doi.org/10.1016/j.immuni.2014.06.008
Naksuriya O, van Steenbergen MJ, Torano JS, et al (2016) A Kinetic Degradation Study of Curcumin in Its Free Form and Loaded in Polymeric Micelles. AAPS J 18:777–787. https://doi.org/10.1208/s12248-015-9863-0
Paladugulu DV, Kizhakkanoodan KS, Guru BR (2025) Nanosystems for pharmaceutical applications. In: Nanomedicine in Translational Research. Elsevier, pp 189–207
Pe KCS, Saetung R, Yodsurang V, et al (2022) Triple-negative breast cancer influences a mixed M1/M2 macrophage phenotype associated with tumor aggressiveness. PLoS One 17:e0273044. https://doi.org/10.1371/journal.pone.0273044
Praveena J, Guru BR (2021) Simultaneous estimation of paclitaxel and curcumin in nano-formulation: Stability analysis of drugs, optimization and validation of HPLC method. J Appl Pharm Sci 11:071-083,. https://doi.org/10.7324/JAPS.2021.110308
Praveena J, Hakkimane SS, Guru BR (2022) Synergistic effect of Paclitaxel and Curcumin in nano-formulations on U87 and A549 cancer cell lines. J Appl Pharm Sci 12:31–47. https://doi.org/10.7324/JAPS.2021.120204
Praveena J, Rallapalli Y, Kizhakkanoodan KS, et al (2025) Dual drug delivery of Paclitaxel and Curcumin via hyaluronic acid functionalized nanoparticles for improved breast cancer therapy. J Biomater Sci Polym Ed 36:2677–2700. https://doi.org/10.1080/09205063.2025.2525668
Pu J, Guardia CM, Keren-Kaplan T, Bonifacino JS (2016) Mechanisms and functions of lysosome positioning. J Cell Sci 129:4329–4339. https://doi.org/10.1242/jcs.196287
Qian B-Z, Pollard JW (2010) Macrophage diversity enhances tumor progression and metastasis. Cell 141:39–51. https://doi.org/10.1016/j.cell.2010.03.014
Raschke WC, Baird S, Ralph P, Nakoinz I (1978) Functional macrophage cell lines transformed by Abelson leukemia virus. Cell 15:261–7. https://doi.org/10.1016/0092-8674(78)90101-0
Roshan Z, Haddadi-Asl V, Ahmadi H, Moussaei M (2024) Curcumin-Encapsulated Poly(lactic- *co* -glycolic acid) Nanoparticles: A Comparison of Drug Release Kinetics from Particles Prepared via Electrospray and Nanoprecipitation. Macromol Mater Eng 309:. https://doi.org/10.1002/mame.202400040
Schieber M, Chandel NS (2014) ROS Function in Redox Signaling and Oxidative Stress. Current Biology 24:R453–R462. https://doi.org/https://doi.org/10.1016/j.cub.2014.03.034
Shiri S, Alizadeh AM, Baradaran B, et al (2015) Dendrosomal curcumin suppresses metastatic breast cancer in mice by changing m1/m2 macrophage balance in the tumor microenvironment. Asian Pac J Cancer Prev 16:3917–22. https://doi.org/10.7314/apjcp.2015.16.9.3917
Steenbrugge J, Breyne K, Demeyere K, et al (2018) Anti-inflammatory signaling by mammary tumor cells mediates prometastatic macrophage polarization in an innovative intraductal mouse model for triple-negative breast cancer. J Exp Clin Cancer Res 37:191. https://doi.org/10.1186/s13046-018-0860-x
Tang M, Chen B, Xia H, et al (2023) pH-gated nanoparticles selectively regulate lysosomal function of tumour-associated macrophages for cancer immunotherapy. Nat Commun 14:5888. https://doi.org/10.1038/s41467-023-41592-0
Wang N, Feng T, Liu X, Liu Q (2020) Curcumin inhibits migration and invasion of non-small cell lung cancer cells through up-regulation of miR-206 and suppression of PI3K/AKT/mTOR signaling pathway. Acta Pharm 70:399–409. https://doi.org/10.2478/acph-2020-0029
Wang YJ, Pan MH, Cheng AL, et al (1997) Stability of curcumin in buffer solutions and characterization of its degradation products. J Pharm Biomed Anal 15:1867–76. https://doi.org/10.1016/s0731-7085(96)02024-9
Weagel EG, Smith CD, Liu P, et al (2015) Macrophage Polarization and Its Role in Cancer. J Clin Cell Immunol 6:1–8
Wu T, Liao Y (2025) Roles of tumor-associated macrophages in triple-negative breast cancer progression. Front Immunol Volume 16-2025: https://doi.org/10.3389/fimmu.2025.1677363

Yallapu MM, Jaggi M, Chauhan SC (2012) Curcumin nanoformulations: a future nanomedicine for cancer. Drug Discov Today 17:71–80. https://doi.org/10.1016/j.drudis.2011.09.009
Yin L, Duan J-J, Bian X-W, Yu S-C (2020) Triple-negative breast cancer molecular subtyping and treatment progress. Breast Cancer Res 22:61. https://doi.org/10.1186/s13058-020-01296-5
Yunna C, Mengru H, Lei W, Weidong C (2020) Macrophage M1/M2 polarization. Eur J Pharmacol 877:173090. https://doi.org/10.1016/j.ejphar.2020.173090
Zhao F, Gong Y, Hu Y, et al (2015) Curcumin and its major metabolites inhibit the inflammatory response induced by lipopolysaccharide: translocation of nuclear factor-κB as potential target. Mol Med Rep 11:3087–93. https://doi.org/10.3892/mmr.2014.3079
Zhukova V, Osipova N, Semyonkin A, et al (2021) Fluorescently labeled plga nanoparticles for visualization in vitro and in vivo: The importance of dye properties. Pharmaceutics 13:. https://doi.org/10.3390/pharmaceutics13081145

Supplementary Files

This is a list of supplementary files associated with this preprint. Click to download.

- SupplementaryeditedNOV17.docx